Contrib Mineral Petrol (1989) 102:492–513

Contributions to Mineralogy and Petrology

Diffusive crystal dissolution

Youxue Zhang*, David Walker, and Charles E. Lesher
Lamont-Doherty Geological Observatory and Department of Geological Sciences of Columbia University, Palisades, New York, NY 10964, USA

Abstract. Crystal dissolution may include three component processes: interface reaction, diffusion and complications due to convection. We report here a theoretical and experimental study of crystal dissolution in silicate melt without convection. A reaction-diffusion equation is developed and numerically solved. The results show that during non-convective crystal dissolution in silicate melt, the interface melt composition reaches a constant or stationary "saturation" composition in less than a second, hence interface reaction is not the rate-determining step and crystal dissolution in silicate melt is usually diffusion-controlled. Crystal dissolution experiments (designed to suppress convection) show that the concentration profiles of all components propagate into the melt according to the square root of run duration, and that the dissolution distance is also proportional to the square root of run duration. Thus our experiments confirm that the dissolution is diffusion controlled, which is consistent with our numerical calculations. For some principal equilibrium-determining components, concentration profiles conform approximately to the analytical solution of the diffusion equation with a constant effective binary diffusion coefficient. Diffusive dissolution rates (which are inversely proportional to square root of time) can thus be predicted from the phase equilibria and the effective binary diffusion coefficients. To predict steady-state convective dissolution rates, the thickness of the boundary layer must be known. If the convective compositional boundary layer thickness around a dissolving crystal aggregate or near the wall of a magma chamber during convection is about 2 cm or larger, then convective dissolution would rarely result in any significant alteration of original melt. Our dissolution experiments also illustrate the complexity of the diffusion process. Uphill diffusion is common, especially during olivine dissolution into andesitic melt where a majority of the components show the effect of diffusion up their own concentration gradients. Uphill diffusion has implications to the understanding of crystal zoning, and suggests caution is required in applying least squares mass balance analysis to magmatic rocks affected by processes involving diffusion.

* *Present address:* Division of Geological and Planetary Sciences, 170-25, California Institute of Technology, Pasadena, CA 91125, USA

Offprint requests to: D. Walker

Introduction

An understanding of the processes by which crystals dissolve is necessary for the study of many geological processes, such as the partial melting of mantle and crustal rocks, and the subsequent contamination of these magmas once they leave their source region. Previous studies of crystal dissolution encompass both theoretical and experimental approaches. Kirkpatrick (1975), Dowty (1980), and Kirkpatrick (1981) reviewed the theoretical background of crystal growth, much of which can also be applied to crystal dissolution. Two processes, reaction at the crystal-melt interface and diffusion in the melt (or in the crystal), happen simultaneously during non-convective crystal dissolution. The dissolution rate (or the growth rate) may be controlled by either interface reaction or diffusion. If the reaction at the crystal-melt interface is slow compared to diffusion in the melt (or crystal), or no diffusion is necessary, the process is controlled by the rate of interface reaction; otherwise, if diffusion in the melt (or the crystal) is necessary and is slow compared to the attachment and detachment of atoms at the interface, the process is controlled by diffusion. The coupling of interface reaction and diffusion makes it very difficult to analytically treat even the non-convective crystal dissolution (or growth) problem. Lasaga (1982) was the first to consider the coupling of interface reaction and diffusion through a crystal growth equation in which the growth rate (or interface reaction rate) was related to time or interface concentration. (Prior to Lasaga 1982, analytical treatment of crystal dissolution either assumed constant growth rate or used a Stephan approach, i.e., $t^{-1/2}$ dependence of growth rate.) Lasaga obtained a solution for the interface composition in the form of an integral equation by using a Laplace transform with respect to x (instead of t as in the usual approach). The solution can be applied to any system if the growth rate can be written as a function of melt composition.

Experimental studies of crystal dissolution have been conducted by Watson (1982a); Tsuchiyama and Takahashi (1983); Harrison and Watson (1983, 1984); Donaldson (1985); Kuo and Kirkpatrick (1985); Marvin and Walker (1985); Tsuchiyama (1985a, b); Brearley and Scarfe (1986). Among them, Tsuchiyama and Takahashi (1983), Marvin and Walker (1985) and Tsuchiyama (1985a, b) examined the kinetics of partial melting at the mutual boundary of

two crystals or of crystal dissolution into finite melt reservoirs. These studies differ significantly from what we will report in this paper and will not be discussed further. Watson (1982a) determined experimental dissolution rates of quartz, feldspar, and a synthetic granite in basaltic melt. He noted uphill diffusion and addressed its significance in the selective contamination of mantle-derived magmas. Donaldson (1985) determined the dissolution rates of olivine, plagioclase and quartz in basaltic melt. Kuo and Kirkpatrick (1985) studied the dissolution rate of forsterite, diopside, enstatite, and quartz in the system $Di-Fo-SiO_2$ at 1 atmosphere. They all found that the dissolution rate was time-independent (explained by free convection in the experimental charge) and independent of crystallographic orientation. Harrison and Watson (1983, 1984) investigated the kinetics of zircon and apatite dissolution in felsic melt. Brearley and Scarfe (1986) studied dissolution of natural olivine, pyroxene, spinel, and garnet in a natural alkali basaltic melt and found concentration profiles to be time-independent and concluded also that the dissolution rate was time-independent. They also tried to obtain diffusivities from their steady-state concentration profiles and found that the diffusivities thus obtained depend not only on temperature and pressure, but also on the dissolution rate.

All the above experimental studies, with the exception of Harrison and Watson (1983, 1984), have examined crystal dissolution where convection operated in the melt. Convection leads to the constant dissolution rates and to the development of steady-state concentration profiles, as obtained by Watson (1982a), Kuo and Kirkpatrick (1985) and Brearley and Scarfe (1986). These dissolution rates can be applied to natural systems only if the convection regimes in natural and experimental systems are similar.

We report in this paper studies of crystal dissolution which address non-convective crystal dissolution. We first evaluate the relative importance of interface reaction through numerical solution of the reaction-diffusion equation. We then examine the diffusive aspect of crystal dissolution both by analytical solution to the diffusion equation and by experiments designed to suppress convection. Finally we apply our results by extrapolation to natural magmatic systems, where convection is usually present and complicates dissolution.

Interface reaction

Two processes occur simultaneously during non-convective crystal dissolution into a melt of different composition. Interface reaction, the attachment and detachment of atoms at the crystal-melt interface, determines the intrinsic maximum dissolution rate. Meanwhile, diffusion, the transport of mass to and from the interface, determines whether this maximum rate can be attained. Because diffusion rates influence interface composition which, in turn, determines the degree of saturation at the interface and thus the interface reaction rate, the two processes are coupled and it is their interplay that controls dissolution. It is important, therefore, to ascertain the conditions under which one or the other of these two processes controls the dissolution rate.

In order to examine the relative roles of reaction at the crystal-melt interface and diffusion in the melt, a reaction-diffusion equation is developed which treats both interface reaction and diffusion in the melt simultaneously. The equation is then solved numerically to evaluate the relative importance of interface reaction and diffusion for magmatic conditions. This approach differs from that of Lasaga (1982) in that we relate the reaction rate to diffusion through the degree of saturation at the interface so that we can determine the relative roles of interface reaction and diffusion in a general way. However, mathematically, our numerical solution can be viewed as a special case of Lasaga's master solution.

The strategy to develop a reaction-diffusion equation is as follows: First the interface reaction rate equation is expressed in terms of the degree of saturation at the interface. Then the degree of saturation of the melt (including interface melt) is shown to satisfy a diffusion equation if deviation from equilibrium is not great.

The interface reaction rate for continuous dissolution can be expressed as (e.g., Kirkpatrick 1981):

$$V_s = f a_0 \nu e^{-\Delta G_a/RT}(e^{-\Delta G_c/RT} - 1) \tag{1}$$

where V_s is the crystal dissolution rate, ΔG_a and ν are the activation energy and vibrational frequency of the activated transition complex, ΔG_c is the difference in partial molar free energies of the dissolving species between liquid and crystalline states, f is the fraction of sites available, a_0 is the distance between subsequent layers of the crystal, R is the gas constant and T is the temperature in Kelvin. Notice this equation is different from the equation for crystal growth by a negative sign. The crystal dissolution rate V_s in (1) refers to the rate at which a fixed point in the crystal moves relative to the crystal-melt interface. However, when discussing diffusion in the melt it is important to establish the rate at which the interface moves relative to the melt (or a fixed point in the melt). This rate is hereafter referred as the melt growth rate. To dissolve a crystal layer of some thickness, a thicker layer of melt will be produced if the crystal is denser than the melt. As such, the melt growth rate exceeds than the crystal dissolution rate. Specifically the melt growth rate differs from the crystal dissolution rate by a constant equal to the ratio of crystal density over melt density. Multiplying both sides of (1) by this density ratio transforms the crystal dissolution rate into the melt growth rate (denoted as V).

The degree of saturation (denoted as w) is defined as:

$$w = e^{\Delta G_c/RT} \tag{2}$$

where the exponential term is analogous to chemical affinity of reaction (Denbigh 1966). w is a function of melt composition which varies with distance away from the interface. It may also refer to the degree of metastable saturation (possible metastable saturation will be discussed later). For simplicity, "saturation" or "equilibrium" (with quotation marks) is used in this sense to include the case for metastable equilibrium. Now by defining:

$$V_a(T) = h f a_0 \nu e^{-\Delta G_a/RT} \tag{3}$$

where h is the ratio of the crystal density over melt density, and by substituting (2) and (3) into (1), we can write:

$$V = V_a\left(\frac{1}{w_0} - 1\right) \tag{4}$$

where w_0 is the degree of "saturation" at the interface. V_a in (4) is a function of temperature but is assumed to be independent of w_0. At a fixed temperature w can be written as a function of the concentrations of the participating com-

ponents:

$$w=f(C_1, C_2, \ldots, C_n) \tag{5}$$

which can be linearly approximated near the "equilibrium" state by:

$$w \approx 1+\sum_{i=1}^{n} k_i(C_i-C_i^e)=\left(\sum_{i=1}^{n} k_i C_i\right)-A \tag{6}$$

The superscript "e" indicates the concentration at "equilibrium" and A and k_i's are constants at fixed temperature. At constant temperature we have:

$$\frac{\partial w}{\partial t} \approx \sum_{i=1}^{n} k_i \frac{\partial C_i}{\partial t} \tag{7}$$

The diffusion equation for component i during planar dissolution in an interface-fixed reference frame can be written as:

$$\frac{\partial C_i}{\partial t}=\frac{\partial}{\partial x}\left(D_i \frac{\partial C_i}{\partial x}\right)-V\frac{\partial C_i}{\partial x} \tag{8}$$

where x is the distance in the melt away from the interface, D_i is the diffusivity of component i, and V is the melt growth rate. Combining (7) and (8) gives:

$$\frac{\partial w}{\partial t}=\frac{\partial}{\partial x}\left(\bar{D}\frac{\partial w}{\partial x}\right)-V\frac{\partial w}{\partial x} \tag{9}$$

where

$$\bar{D}=\frac{\sum_{i=1}^{n} D_i k_i \frac{\partial C_i}{\partial x}}{\sum_{i=1}^{n} k_i \frac{\partial C_i}{\partial x}} \tag{10}$$

$\bar{D}$ in (10) is a weighted average of D_i in (8) and can be regarded as an effective binary diffusion coefficient (EBDC). Using EBDC is a simplified approach in describing multicomponent diffusion by treating all other components in the system as one "component" and hence reducing the system to effective binary or pseudobinary (Cooper 1968; Hofmann 1980) when complete diffusion data are not available.

The complete reaction-diffusion equation sought in this section consists of the following set of equations: Eq. (9), where V is defined by (4), with the following initial and boundary conditions[1]:

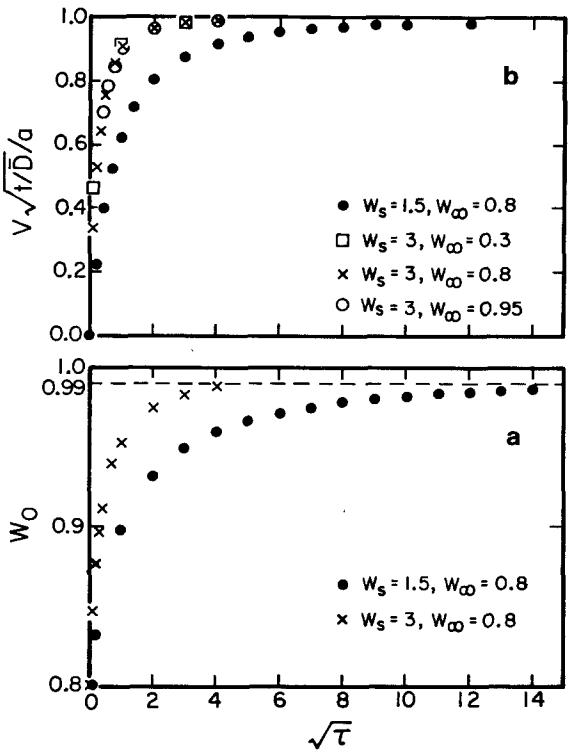

Fig. 1a, b. Evolution of the degree of saturation at the interface and the dissolution rate. **a** degree of saturation at the interface vs dimensionless time; **b** dissolution rate vs time. **Fig. 1b** is essentially the same as **a** but it shows how $V\sqrt{t}$ reaches a constant. The constant a is calculated from Eq. (3) by replacing C with w. The constant is used to scale the vertical variable so that it approaches 1 as time increases

initial condition: $w|_{t=0}=w_\infty \quad x>0$ (11a)

boundary condition at $x=\infty$: $w|_{x=\infty}=w_\infty \quad t>0$ (11b)

boundary condition at $x=0$:

$$\bar{D}\frac{\partial w}{\partial x}\bigg|_{x=0}-V(w|_{x=0}-w_s)=0 \quad t>0 \tag{11c}$$

where w_∞ is the initial degree of "saturation" of the melt, and w_s is the degree of "saturation" of a melt whose composition is the same as that of the crystal (see Table 1 for the calculation). Condition (11b) requires that the melt reservoir is "infinite" compared to the diffusion distance.

The reaction-diffusion equation can be made dimensionless by replacing x and t with $V_a x/\bar{D}$ and $V_a^2 t/\bar{D}$ respectively. Assuming V_a and $\bar{D}$ are constant, it can be solved numerically given values for w_s and w_∞ using either Lasaga's (1982) method or an algorithm to solve a differential equation. Results of the numerical calculations are shown in Fig. 1, which plots the evolution of the degree of "saturation" at the interface and the scaled dissolution rate $V\sqrt{t/\bar{D}}/a$ as a function of dimensionless time $\tau(=V_a^2 t/\bar{D})$. Because the relative precision of electron microprobe analyses is usually no better than 1% for most of the major oxide components of a glass sample, for all practical purposes, the interface composition can be regarded at "saturation" when $w|_{x=0}$ exceeds 0.99 (see Fig. 1a). Likewise, when $V\sqrt{t/\bar{D}}/a$ exceeds 0.99, (i.e. $V \approx a\sqrt{\bar{D}/t}$) the dissolution rate can be regarded as inversely proportional to the square root of time, implying that crystal dissolution is totally diffusion-controlled

[1] The reaction-diffusion equation at variable temperature which is a function of time can be written as:

$$\frac{\partial w}{\partial t}=\frac{\partial}{\partial x}\left(\bar{D}\frac{\partial w}{\partial x}\right)-V\frac{\partial w}{\partial x}+\sum_{i=1}^{n} C_i\frac{\partial k_i}{\partial t}-\frac{\partial A}{\partial t} \quad x>0, \quad t>0$$

where V is given by (4) and initial and boundary condition at $x=0$ are the same as (11). The boundary condition at $x=\infty$ is:

$$w|_{x=\infty}=\left(\sum_{i=1}^{n} k_i C_i|_{x=\infty}\right)-A$$

where $C_i|_{x=\infty}$ is a constant; but k_i's and A are not. This reaction-diffusion equation can be solved numerically given temperature as a function of time and V, A, and k_i's as a function of temperature

Table 1. Parameter w_s[a] of some minerals at different temperatures

T (° C)	1200	1300	1400	1500	Liquidus (° C)
OL(FO90)	4.3	3.0	2.2	1.6	1770
DIOP	2.4	1.5	m[b]	m	1391
PL(AN60)	1.9	1.4	m	m	1333

[a] Calculated w_s is from the 1 atm basaltic melt saturation surface and the composition of a melt whose composition is the same as the crystal. (w_s at higher pressure is higher.) For example, w_s for olivine is calculated from:

$$w_s=\frac{K_d^{MgO}(MgO^{OL}+0.3\ FeO^{OL})}{66.67}$$

where MgO^{OL} and FeO^{OL} are MgO and FeO cation mole percent in olivine and K_d^{MgO} is the simple partition coefficient of MgO between olivine and melt. The effect of SiO_2 on w has been ignored. Calculations used experimental data summarized in Weaver and Langmuir (in press)

[b] m means the crystal melts at the temperature

(Fig. 1b). The period before $V\sqrt{t/\bar{D}}/a$ reaches 0.99 is hereafter called the initiation period and the time at which this is satisfied is defined as the critical time. From the dimensionless critical time (denoted as τ^*) inferred from Fig. 1b we can calculate the real critical time (denoted as t^*) in seconds if V_a and $\bar{D}$ are known. Further, from Fig. 1b it is seen that the critical time depends on w_s but is insensitive to w_∞ (although the diagram shows only the cases where $w_\infty \leq 0.95$, our result shows that the critical time at $w_\infty = 0.9999$ is similar to that at $w_\infty = 0.95$). As w_s decreases, the initiation period increases. Consider the case for $w_s \geq 1.5$ (see Table 1 for values of w_s for basaltic melts), the dissolution is totally diffusion controlled at $\tau \geq 200$. For a V_a of 0.034 cm/s appropriate for diopside (calculated from data of diopside dissolution in its own melt at 1393°–1412° C, Kuo and Kirkpatrick 1985), and $\bar{D}$ between 10^{-9} and 10^{-6} cm^2/s at magmatic temperatures (Hofmann 1980), the real critical time t^*, corresponding to $\tau^* = 200$, is 0.0002 to 0.2 s. Hence the real critical time, representing the amount of time necessary for dissolution to become effectively diffusion controlled, is a trivial time interval at either laboratory or natural conditions. If the values of V_a for other crystals are comparable in magnitude to that of diopside (certainly this warrants more investigation), it may be generally concluded that the interface composition reaches a constant or stationary "saturation" composition in less than a second and that dissolution thereafter will be essentially diffusion controlled. Only when V_a is very small (less than one hundredth that for diopside), or w_s is very close to 1 (i.e., at a temperature near the liquidus of the dissolving crystal), or D is 10^4 times greater, will the initiation period be long enough to be important and measurable. This analysis demonstrates that the common assumption that the interface melt is near "saturation" during dissolution is valid under most circumstances. Therefore the driving force for crystal dissolution is the very small undersaturation which usually is not directly measurable. This is because the parameter V_a is very large (i.e., the dissolution rate of a crystal into its own melt is very large) and the diffusivity is very small. If a crystal dissolves into its own melt, heat conduction and interface reaction happen simultaneously. Replacing chemical diffusivity by the thermal diffusivity κ which is about 0.01 cm^2/s, it can be estimated that the critical time for the dissolution to be controlled by heat conduction is about 30 min. The characteristic thermal diffusion distance during this time is ~ 4 cm. Therefore if the experimental duration is shorter than 30 min or if the charge is smaller than 4 cm along the direction of heat conduction, dissolution is not controlled by heat conduction.

There are two important assumptions we have made in deriving the reaction-diffusion equation and in producing our numerical results. The first is the linear dependence of the degree of saturation on melt composition, Eq. (6), and the second is the treatment of diffusion in the melt as effectively binary although $\bar{D}$ is for a multicomponent species. To take a more rigorous approach, detailed information about the saturation surfaces and the diffusion coefficient matrices would be required, which is not available at present. One would think that the assumption of $\bar{D}$ being approximately constant is not valid because included in $\bar{D}$ are some components that may diffuse uphill. This question will be addressed later using experimental results (Fig. 15) and it will be shown that w can be approximately described by effective binary diffusion. We believe that additional constraints on non-linearity and cross-term diffusion will not change our qualitative conclusion that crystal dissolution rate is diffusion controlled under realistic laboratory and natural time scales for dissolution. Experimental results presented in later sections confirm that diffusion is the controlling mechanism for moderately superheated dissolution when convection is suppressed.

The mass transport rate during convective dissolution is usually faster than during diffusive dissolution. Interface reaction might become the rate-limiting step if vigorous convection leads to a very thin boundary layer. However, this would occur only when the characteristic diffusion distance ($\sqrt{\bar{D}t^*}$) is reduced to 0.5 μ or less since $\sqrt{\bar{D}t^*}$ (where t^* is the critical time) is about 0.5 μ. The development of such a thin boundary layer would require very vigorous convection difficult to achieve in either laboratory or natural settings. Thus interface reaction is usually not the rate-determining step during convective dissolution as well.

Analytical solution to diffusive crystal dissolution

Having established that non-convective crystal dissolution is diffusion controlled, it is now instructive to obtain analytical solutions for diffusive crystal dissolution. In an interface-fixed reference frame, binary diffusion in melt adjacent to a dissolving crystal can be written as:

$$\frac{\partial C}{\partial t}=\frac{\partial}{\partial x}\left(D\frac{\partial C}{\partial x}\right)-V\frac{\partial C}{\partial x} \qquad x>0, \quad t>0 \tag{12a}$$

$$\text{where} \quad V=a\sqrt{\frac{D}{t}}, \quad \text{and hence} \quad L=2a\sqrt{Dt} \tag{12b}$$

$$\text{with the initial condition:} \quad C|_{t=0}=C_\infty, \qquad x>0 \tag{12c}$$

and the boundary conditions:

$$\text{at } x=\infty: \quad C|_{x=\infty}=C_\infty, \qquad t>0 \tag{12d}$$

$$\text{at } x=0: \quad D\left.\frac{\partial C}{\partial x}\right|_{x=0}-V(C|_{x=0}-C_s)=0, \qquad t>0 \tag{12e}$$

where C is the concentration of a given component, C_∞ is the initial concentration, C_s is the concentration in the

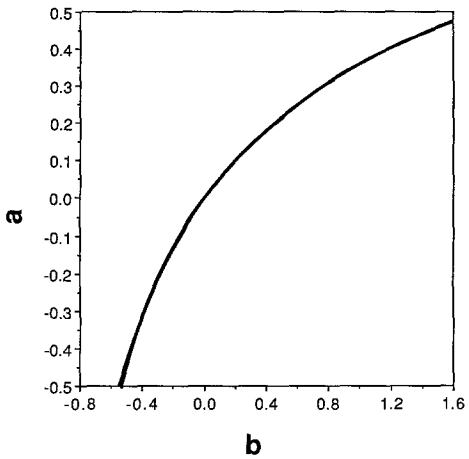

Fig. 2. Plot of a vs b where $b=\sqrt{\pi}\,a e^{a^2}\,\mathrm{erfc}(-a)$

crystal, D is the binary diffusion coefficient, V is the melt growth rate and L is the melt growth distance. Equation (12a) can be transformed to an ordinary differential equation using the Boltzmann transformation (Crank 1975), i.e. replacing both x and t by a single variable $\eta(=x/2\sqrt{t})$, which is possible because V is inversely proportional to the square root of t. Therefore concentration versus $x/\sqrt{t}$ should be time-independent, implying that concentration profiles propagate into melt according to the square root of time regardless of the compositional dependence of the diffusion coefficient. The solution of (12) for constant D is:

$$\frac{C-C_\infty}{C_0-C_\infty}=\mathrm{erfc}\left(\frac{x}{2\sqrt{Dt}}-a\right)\Big/\mathrm{erfc}(-a) \tag{13}$$

where C_0 is concentration at the interface (assumed to achieve a stationary concentration in less than one second as established in the previous section), and the parameter a satisfies:

$$\sqrt{\pi}\,a e^{a^2}\,\mathrm{erfc}(-a)=b \tag{14a}$$

where

$$b=\frac{C_0-C_\infty}{C_s-C_0} \tag{14b}$$

The relationship between a and b is plotted in Fig. 2.

In a multi-component system the binary diffusion coefficient D can be replaced by an effective binary diffusion coefficient (EBDC) for any component which can be approximately characterized by effective binary diffusion, yielding relations analogous to Eq. (12) through (14). However, the diffusional behavior of some components, for instance, the alkalies during quartz and feldspar dissolution into basaltic melt (Watson 1982a), cannot be described by effective binary diffusion with constant EBDC's. In such cases the above solutions are not applicable. The diffusion equation for such a component includes non-negligible cross terms due to the effects of other components. However, because of the inverse relationship of melt growth rate to the square root of time, it can be shown that the diffusion equation for such a component can also be parameterized by $\eta=x/2\sqrt{t}$ (even if every element in the diffusion coefficient matrix depends on concentration), and therefore, the concentration profile should still propagate into melt according to square root of time[2].

Relations (12) and (14) permit us to predict diffusive dissolution rates if we know initial melt and crystal composition, the interface melt composition and the diffusion coefficient. In particular, we can qualitatively predict the relative diffusive dissolution rates for various minerals if we assume EBDC's do not vary significantly during the dissolution process. Because the dissolution rate is proportional to a and a varies positively with b (Fig. 2), crystal dissolution rates increase with b. Therefore, increasing $|C_s-C_0|$ or decreasing $|C_0-C_\infty|$ will decrease the dissolution rate. If the compositional "difference" between the mineral and the interface melt is larger at similar C_0, b will be smaller, thus the dissolution rate will be smaller. For this reason, a pure forsterite is expected to dissolve more slowly in a basaltic melt than Fo90 or Fo70. (Intuitively, during pure forsterite dissolution it is more difficult to transport the excess MgO away from the interface and hence the dissolution rate is slower.) Comparisons between pyroxene and olivine dissolution rates are more difficult because there are significant differences in the interface compositions at the same temperature (i.e. a difference in the numerator of b). However, pyroxene compositions are much closer to basaltic compositions than olivine; thus the denominator terms often dominate the b parameter. As such the dissolution rates of pyroxenes in basaltic melt are often greater than those of olivines except at temperatures close to the pyroxene saturation temperature where C_0-C_∞ becomes very small and controls the value of b. Therefore, at low pressures and at *moderate undersaturation*, mineral dissolution rates will follow the following order:

Opx, cpx, plag > olivines, spinels
> accessory minerals (apatite, zircon, etc.) (15a)

In cases involving solid solutions:

intermediate members > pure end members (15b)

At first glance these predictions for dissolution rates may seem counterintuitive. One might suppose that the driving forces for crystal dispersal would be dependent on the chemical differences between melt and crystals, but our analytical results highlight the importance of solubility in modifying this expectation. Thus zircon is slow to dissolve in silicate melts because of its low solubility as shown by Harrison and Watson (1983).

Experimental procedures and analytical methods

Experiments to examine dissolution of crystals (San Carlos olivine, synthetic pure forsterite, diopside, spinel, quartz and rutile) in a natural andesite melt were performed under controlled laboratory

[2] If the diffusion coefficient matrix for a multi-component system is constant, the solution to Eq. (12) can be applied to each "eigen" vector in composition space (Cooper 1974) with D being replaced by an eigen value of the diffusion coefficient matrix. Therefore the concentration of any component i in the melt is a combination of the solution for the "eigen" vectors, namely:

$$C_i=C_{i\infty}+\sum_{j=1}^{n}u_{ij}\,\mathrm{erfc}\left(\frac{x-L}{2\sqrt{\lambda_j t}}\right)\Big/\mathrm{erfc}\left(\frac{-L}{2\sqrt{\lambda_j t}}\right)$$

Therefore the concentration profile for component i propagates into melt according to square root of time

Table 2. Starting compositions

	LML DCP[a]	LML[b] Probe	Oliv[c] Probe	Fors Probe	Diop Probe	Sp Probe	Qtz Probe	Rt Probe
SiO_2	56.1	56.5	40–41	42.7	55.2	0.02	99.92	0.1
TiO_2	1.18	1.24	0	0	0.01	0.01	0	99.2
Al_2O_3	17.7	18.0	0.03	0	0.37	71.2	0.03	0.5
FeO	7.03	6.71	8–11	0.3	0.65	0.82	0.01	0.2
MgO	3.93	3.96	48–51	56.8	17.63	27.5	0	0.05
MnO	0.127	0.13	0.15	0	0.08	0.1	0	0
CaO	7.51	7.73	0.1	0	25.57	0	0	0
Na_2O	3.86	3.75	0	0	0.23	0	0	0
K_2O	1.70	1.7	0	0	0	0	0	0
P_2O_5	0.39	0.38	0	0	0	0	0.01	0
Sum	99.5	100.1	–	99.8	99.74	99.65	99.97	100.1

[a] Unpublished Lamont data for natural rock powder (LML 30-1) by DC plasma analysis
[b] Electron microprobe analysis on glass prepared from rock powders
[c] San Carlos olivine composition is variable, Fo88-91

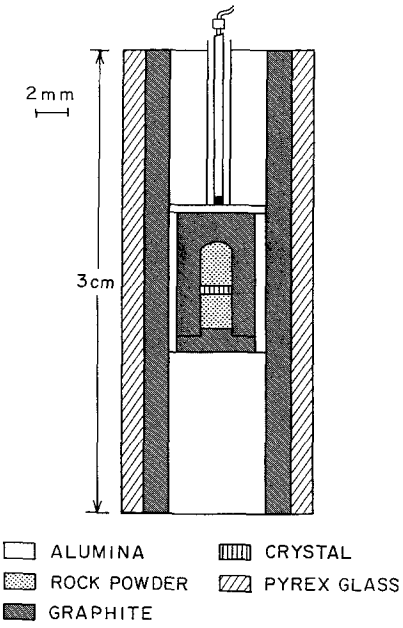

Fig. 3. Sketch of the experimental configuration within a 1/2″ piston cylinder pressure vessel

conditions. The compositions of starting materials are listed in Table 2.

Dissolution experiments

All experiments were run at 5–23 kb in a piston-cylinder apparatus to insure good crystal-melt contact and to prevent melt vesiculation. Figure 3 depicts our experimental geometry, which insures that diffusion is one-dimensional, that at least one side is convection-free due to gravitational stability, and that a negligible amount of melt exchanges between the two sides of the crystal due to the tight fit of the crystal wafer in the capsule. A natural andesite rock powder was fused twice at 1300° C and 1 bar QFM for ~2 h to produce glass starting material. Crystal grains were sawed into wafers 200–1000 μ thick (no attention was paid to crystallographic orientation). The wafers were then ground into cylindrical disks 2 mm in diameter which fit tightly into graphite capsules 9.5 or 6.5 mm long. Capsule length was dictated by run duration to insure that the melt reservoir was effectively infinite compared to the developing diffusion profiles. When possible, a shorter capsule was used to minimize temperature differences within the experimental charge. The disks were horizontally oriented and packed with vitreous rock powder (to be remelted during the experiment) on one side or both sides. The capsules were enclosed in alumina sleeves and then encased in a 3 cm long graphite heater of ~0.64 cm inner diameter. Pyrex glass served both as the pressure medium and to insulate the furnace from the carbide core.

Table 3 lists the run conditions for our crystal dissolution experiments. Run pressures reported in Table 3 are nominal pressures with "piston-out" procedure initially over-pressurized to ~15 kb for 5 kb runs and by ~5 kb for runs at higher pressures. Run temperatures were monitored and controlled by a Pt-Pt90Rh10 thermocouple input to a Eurotherm 984 control system. Temperature fluctuations in the charge during a run were usually ±0.5° C once the stable running temperature was reached, which usually took ~30 s. The temperature difference from center to bottom of the charge inside the capsule was calibrated by measuring interface melt composition of olivines at center and bottom of the charge and using olivine saturation "thermometer" (Roeder and Emslie 1970; Langmuir and Hanson 1981). This difference is ~25° C for the 9.5 mm capsule at run temperature of 1400° C, equivalent to a temperature gradient of ~8° C/mm.

Each charge was quenched to below the solidus of the melt in 1~2 s by shutting off power to the piston-cylinder apparatus. After extraction the charge was mounted in an epoxy disc, ground to reveal the widest axial section, and polished for examination.

Analytical methods

Major element concentrations in the quenched melt and crystal were analyzed using an automated CAMECA electron microprobe at Lamont-Doherty Geological Observatory. The analytical conditions were similar to those of Sack et al. (1987) except that we used a single beam current of 25 nA. When especially good Na_2O analyses were desired, we either used a 5 nA beam current for Na, similar to Sack et al. (1987), or rastered the beam.

One charge was analyzed for trace elements by secondary ion mass spectrometry carried out with the IMS 3f microprobe at MIT. Analytical procedures were similar to those of Lesher (1986) following those set forth in Shimizu and Hart (1982). One exceptionally good Na_2O profile (for # 212, Fig. 7) was analyzed this way.

Experimental results

Figure 4 presents two photomicrographs of an interface between San Carlos olivine and glass (# 212) viewed in reflected light. The interface is nondiffuse and straight. In three dimensional view, the interface must thus be almost perfectly planar. Because about 50 μ of the crystal have

Table 3. Run summary

Run #	T_1	P	T_2	Cryst	Pos	X_i	X_f	ΔX	t (sec)	MgO
212	1290	5.5	1285	OL	Mid	726 ±10	631±2	48 ±5	18000	11.3
216	1290	5.5	1250	OL	Mid	838 ±2	818±10	10 ±5	900	10.05
219	1270	5.5	1250	OL	Bot	802 ±17	725±8	79 ±19	81220	10.05
222	1285	5.5	1302	OL	Bot	510 ±4	470±20	40 ±20	8340	12.15
223	1305	10.5	–	DI	Bot	638 ±20	598±5	40 ±20	4190	8.1
225	1305	10.5	–	DI	Bot	648 ±8	622±7	26 ±11	890	8.0
226	1305	5.5	1285	FO	Bot	373 ±23	345±12	28 ±26	895	11.15
227	1305	5.5	1300	FO	Bot	456 ±9	431±5	25 ±10	8995	12
228	1315	5	1300	OL	Mid	401 ±13	390±3	11 ±13	2400	12.1
228	[a]	[a]	1300	FO	Mid	495 ±13	475±5	20 ±14	[a]	12.1
229	1215	5	1185	OL	Bot	584[c]±25	608±15	−24[c]±29	3600	7.25
231	1365	13	–	OL	Bot	301 ±10	246±6	55[b]±12	1780	13.2
231	1385	[a]	–	SP	Mid	273 ±10	245±5	14 ±6	[a]	5.95
231	1365	[a]	–	DI	Top	1024 ±33	882±10	142[b]±34	[a]	10.8
234	1300	5	–	QT	Top	597 ±13	603±5	− 6 ±14	3600	1.5
235	1350	5	1350	OL	Top	267 ±25	250±5	17 ±25	1100	14.5
236	1375	15	–	OL	Top	260 ±10	157±10	103[b]±14	1800	16.0
236	[a]	[a]	–	RT	Bot	398 ±8	350±20	48 ±22	[a]	4.6
239	1400	5.5	1420	OL	Mid	438 ±10	170±70	134 ±35	4800	19.0
242	1375	21.5	–	DI	Top	428 ±13	372±10	56 ±16	1810	7.7

Note: All the runs used LML 30-1, an andesite rock powder, as starting composition for melt.
T_1 (° C): measured thermocouple temperature with the following two corrections, rounded to the nearest 5° C. One correction is based on the distance of thermocouple junction to the cap of graphite capsule. This correction, however, must be viewed as approximate because the thermocouple junction itself is ~1 mm in diameter and the temperature gradient in that part of the furnace is estimated at 50° C/mm. The second correction is based on the distance of the crystal-melt interface to the center of the capsule (when the capsule is centered in the heater). The temperature gradient inside the capsule is ~8° C/mm at 1400° C
P: measured pressure in kbar
T_2 (° C): temperature calculated from 1 atm olivine saturation surface and interface melt composition assuming interface melt is at saturation. The calculation is only done for 5 kb runs because at this pressure the oversaturation correction (~17° C, see discussion) and the pressure correction (3°–6° C/kb: 3°–4° C from Bender et al. 1978; 5° C on average using data from Ford et al. 1983) almost cancel one another out. At higher pressures, the pressure correction may introduce considerable error. These calculated temperatures may not reflect actual temperatures in the experimental charges as closely as they do relative temperature differences among the different runs
Cryst: Crystal used in experiments, where *OL*=San Carlos olivine, *FO*=synthetic pure forsterite, *DI*=diopside, *SP*=spinel, *QT*=quartz, *RT*=rutile
Pos: crystal position in experimental charge, where *Mid*=Middle and *Bot*=Bottom
X_i: initial thickness of the crystal wafer in microns
X_f: directly measured final thickness of the crystal wafer
ΔX: dissolution distance which is the difference between X_i and X_f (If the crystal wafer is surrounded by melt on both sides, ΔX is half the difference)
t: run duration
MgO: MgO wt% of the interface melt, which indicates the difference of the in situ temperature during dissolution of the same mineral
[a] the same as the above column;
– cannot be determined
[b] There is a small melt reservoir on the other side of the crystal wafer into which part of the crystal has been dissolved. The real ΔX for one side should be smaller
[c] There might be a misreading of the micrometer by 1 grid unit, resulting in a smaller initial thickness by 25 μ

dissolved, the sharpness of the interface at the 1 μ scale is remarkable indicating that the dissolution process is very uniform. Because the interfaces are sharp in the charges we will be discussing, the distance from the interface is well defined except in the presence of cracks.

Many experimental charges cracked subparallel to the crystal-melt interfaces during quench and decompression. The cracks are often in the glass adjacent to the interface. When measuring concentration profiles, it is difficult to estimate the real distance across a crack. In these cases, a number of profiles were measured where the same crack was encountered at different distances from the interface. These profiles were then combined into one composite profile, permitting us to define distance across the crack more accurately.

Quench magnetite crystals of less than 2 μ in dimension are present in most charges. They show good octahedral morphology and are distributed throughout the glassy part of the charge. In some of the olivine dissolution charges magnetite crystals are more concentrated near the olivine-melt interface, possibly due to the high FeO concentrations there.

Dissolution rates

The amount of a crystal wafer dissolved during an experiment was estimated by two methods. The first was a direct measurement of the thickness of the crystal wafer before and after the run. Because of the variability in the thickness of a wafer and uncertainties in measuring this thickness accurately, the errors from direct measurement are usually 5 μ–30 μ which is relatively large compared to the dissolu-

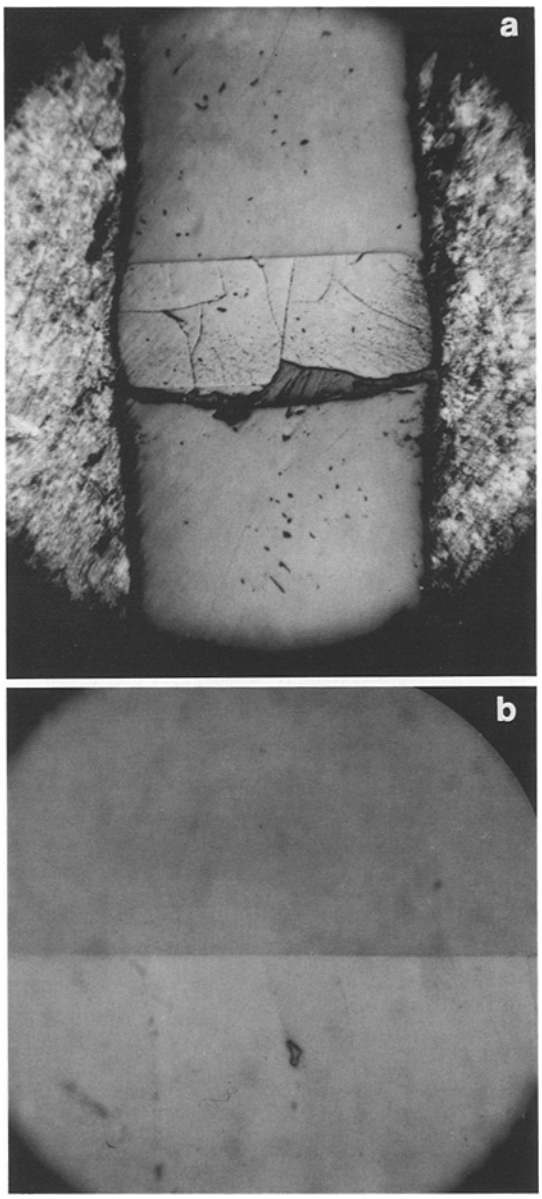

Fig. 4a, b. Photomicrographs of an experimental charge (# 212). **a** whole view of the charge. San Carlos olivine is at the center of the charge. About 3 × 4 mm. **b** a blow up of the interface. Notice the interface is sharp and straight. The width is about 300 μ

tion distance in a given experiment (10 μ–100 μ). The other method for estimating dissolution distances was by mass balance. The excess crystal mass in the glass (melt) was determined from the concentration profile. The mass balance equation is:

$$\int_0^\infty \left(\frac{\rho}{\rho_\infty} C - C_\infty\right) dx = \frac{\rho_s}{\rho_\infty} L_s C_s - L C_\infty \qquad (16)$$

where C and ρ are concentration and density, respectively. The integration is performed over distance x from 0 to infinity. The subscripts "∞" and "s" have the same meaning as those in Eq. (14). L_s is the crystal dissolution distance and L is the glass (melt) growth distance. As we discussed earlier, L differs from L_s by the ratio of the crystal density over glass (melt) density. Because the concentration and distance we measure are those in the glass at room temperature ($\rho_{\text{glass at room temperature}} > \rho_{\text{melt at run temperature}}$), the density in (16) should also be the glass density at room temperature which is not available. We therefore estimate ρ/ρ_∞ from the melt density relationship (Nelson and Carmichael 1979) at run temperature which may not apply exactly. The left hand side of (16) can also be calculated by assuming $\rho/\rho_\infty = 1$ and the maximum error of that term can thus be estimated. For "normal" (i.e. monotonic) profiles, the relative error in this term is usually less than 5%. However, for those profiles which contain minima or maxima, $C - C_\infty$ may change from positive to negative and the integral in (16) can be viewed as the summation of two terms, one positive and one negative. The summation results in a small value for the integral; therefore the relative error is large. Once the left hand side integral term is determined, L_s can be estimated with only small uncertainties if C_∞ is small compared to C_s, and L can be estimated if C_s is small compared to C_∞. All these taken into account, the relative error in estimating L or L_s from "normal" profiles is about 5%–10%, which is better than our direct measurement. Table 4 lists the dissolution distance estimated by the two methods. These estimates agree very well when the relative error in direct measurement is small.

Crystal dissolution distance determined from "normal" concentration profiles is plotted against the square root of run duration for San Carlos olivine, synthetic pure forsterite, and diopside in Fig. 5. The linear dependence of the dissolution distance upon $\sqrt{t}$ demonstrates that the dissolution is diffusion controlled, that convection in the experi-

Table 4. Dissolution distances

Run #	L (meas)	L (MB)	L (calc)
212(OL)	48 ±5	51 ±2	48±5
216(OL)	10 ±2	7.6±0.4	8±1
219(OL)	77 ±19	72 ±4	65±7
222(OL)	40 ±20	45 ±2	47±5
223(DI)	40 ±20	40 ±2	38±4
225(DI)	26 ±11	18 ±1	17±2
226(FO)	26 ±26	10 ±1	12±2
227(FO)	25 ±10	36 ±2	38±4
228(OL)	11 ±13	26 ±2	25±3
228(FO)	20 ±14	24 ±2	23±3
229(OL)	−24 ±29	7 ±1	7±1
231(OL)	55[a]±12	34 ±7	32±10
231(SP)	14 ±11	10 ±0.5	9±0.7
231(DI)	142[a]±34	79 ±2	74±5
234(QT)	18 ±14	15 ±3	18±4
235(OL)	24 ±25	25 ±2	26±4
236(OL)	103 [a]±14	60 ±3	~70
236(RT)	48 ±22	22 ±2	21±2
239(OL)	134 ±35	120 ±5	110±10
242(DI)	56 ±16	47 ±4	48±4

Note: *Run #*: Included in parenthesis is the crystal for which the dissolution distance is measured and near which the profile is considered, where *OL*=San Carlos olivine, *FO*=synthetic pure forsterite, *DI*=diopside, *SP*=spinel, *QT*=quartz, *RT*=rutile; L (meas): directly measured dissolution distance in microns; L (MB): dissolution distance calculated from mass balance; L (calc): dissolution distance calculated from $L = 2a(Dt)^{1/2}/h$

Density used in the calculation: andesitic glass 2.7; olivine and diopside 3.3; spinel 3.58; quartz 2.65; rutile 4.25

[a] The real measured distance should be smaller than that because of a small melt reservoir on the other side which absorbs some crystal thickness

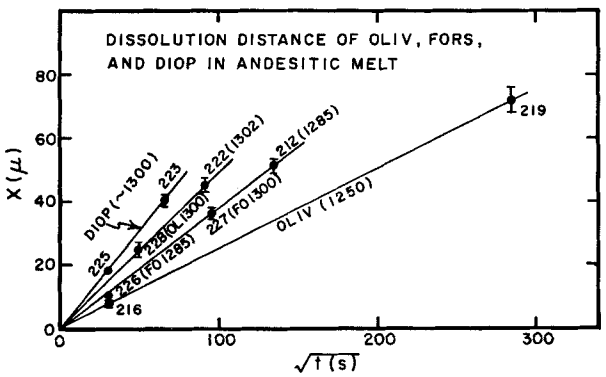

Fig. 5. Dissolution distance vs square root of run duration. In parentheses is calculated temperature (° C), column 4 in Table 3

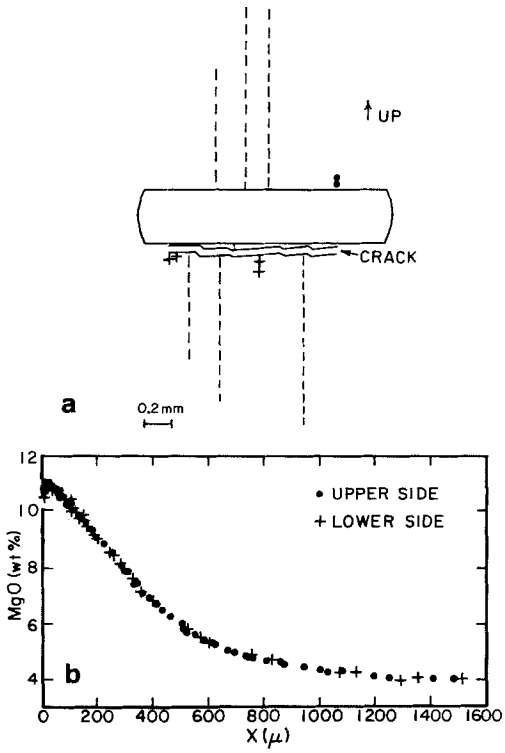

Fig. 6a, b. A detailed MgO concentration profile in the glass of Run # 212 (T = 1285° C, P = 5.5 kb). **a** the distribution of the analyzed points. *Dashed lines* are traverses; a dot is an analyzed single point above the olivine crystal and a cross is a point below the olivine crystal. **b** the concentration profiles of all the analyzed points, including the traverses (*dashed lines* in **a**)

mental charges is suppressed, and that the interface reaction kinetics are not the rate-determining step during crystal dissolution experiments longer than 15 min, consistent with our numerical calculations. From Fig. 5, the dissolution rate (which is inversely proportional to time) of diopside at ~1300° C is greater than that of San Carlos olivine (~Fo90) which, in turn, is slightly greater than that of forsterite at the same temperature. The relative dissolution rates for diopside, olivine, and spinel can also be compared in experiment # 231 (~1375° C and 13 kb). The dissolution rate of diopside is greater than that of olivine, which, in turn, is greater than that of spinel. Finally, the dissolution rate of San Carlos olivine is found to be greater than that of rutile from experiment # 236. All these relations are consistent with our earlier conclusions based upon theoretical considerations (Eq. 15).

Concentration profiles

Two or more profiles perpendicular to an interface were analyzed in each experimental charge. If a crystal wafer has melt on both sides, profiles on both sides of the crystal were measured. Figure 6 includes a schematic diagram of such profiling in one charge (# 212), along with an example for MgO. Figure 6 shows that the experimental charge is horizontally homogeneous: that is, concentration along a line parallel to the interface is constant within error; and that concentration profiles in the melt adjacent to the crystal are symmetric about the crystal. Other experimental charges show similar horizontal homogeneity and symmetry (if both sides are surrounded by melt). Melt on the upper side of olivine crystal (Fig. 6) is gravitationally stable, therefore it does not convect. The symmetry of melt composition about the dissolving olivine suggests that during olivine dissolution into andesitic melt, even the gravitationally unstable side is free of convection. No zonation was detected in the remaining part of the crystals by electron microprobe analysis after the dissolution experiments.

A few of the charges did show horizontal heterogeneity and/or non-symmetry about the crystal. In these charges, bits of graphite were commonly found intruding melt caused by mechanical deformation during the run. If the problem was not severe, we usually characterized the profile in the middle of the charge or away from the visual disturbance, otherwise the run was classified as unsuccessful and not examined further.

An interesting, but disturbing, feature of Fig. 6b is that the compositional profile for MgO bends as it approaches the interface. It occurs in other charges for MgO and in plots of other elements as well, but is most clearly seen for MgO versus distance in olivine dissolution experiments. MgO concentration first increases gradually as the interface is approached, but then decreases suddenly within about 10 μ of the interface. The decrease is not caused by secondary fluorescence within the olivine crystal during microprobe analysis as this would increase (rather than decrease) the MgO concentration. This feature is believed to be a consequence of crystal overgrowths upon the wafer during quench. We have shown numerically that after an initiation period of less than 1 s, the interface melt is essentially at saturation with respect to the crystal; therefore, a decrease in temperature during quench will result in oversaturation with respect to, and hence crystallization of, the crystal that was previously dissolving. Therefore, overgrowths on the crystal will always occur during quench but the amount of growth will depend on the quenching rate, interface reaction rate, the diffusivities and the temperature from which the charge is quenched. (One of the reasons that we chose to use andesitic melt was that the quench effect was small.) MgO is strongly depleted near the interface by olivine overgrowth and is easily observed. By mass balance, a one micron overgrowth of olivine (Fo80) will deplete the glass (melt) within 10 μ by an average of 3.5% MgO. Therefore, the depletion in Fig. 6b can be explained by 0.1 μ–0.2 μ of olivine overgrowth, which is too small a zone to be measured by electron microprobe.

Quench growth complicates the study of zonation profiles in the glass adjacent to a crystal, especially in crystal growth experiments because continuous growth and quench profiles are superimposed and additive. The two differ in that the quench profile is shorter. Crystal dissolution experi-

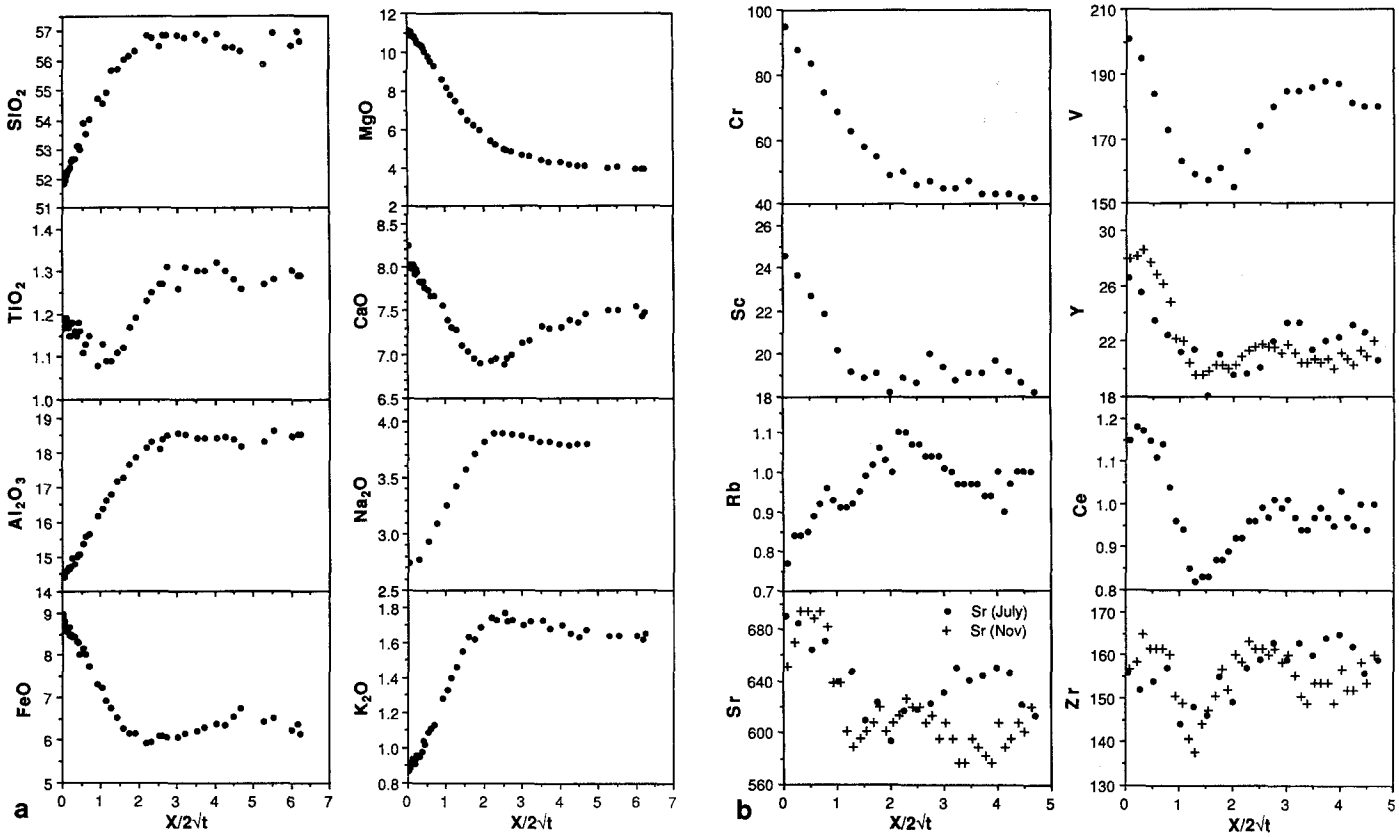

Fig. 7. **a** Major element concentration (wt%) profiles for olivine dissolution into andesitic melt (# 212, T = 1285° C; P = 5.5 kb) vs $x/2\sqrt{t}$ (in $\mu/\sqrt{s}$) in melt where x is distance from crystal-melt interface. Na_2O is analyzed by ion microprobe at MIT. **b** Trace element concentration (ppm) profiles for # 212. Trace elements are analyzed at MIT. Sr, Y and Zr are repeated in two analyses and they are compared in the diagram with date of analysis in parenthesis. Rb and Ce are given in relative concentration where concentration far away is defined to be 1

ments have profiles which are opposing so that the quench phase growth profile is more easily separable from the dissolution profile. But care should be taken in trying to distinguish them.

Because the bend near the interface is not part of the diffusion profile produced during dissolution experiments, we exclude it from subsequent analysis. The term interface composition refers to the melt composition at the interface during dissolution, and is calculated by extrapolation using either a polynomial or visual fit of the diffusion profile not affected by quench.

Figures 7–13 are plots of concentration vs normalized distance ($x/2\sqrt{t}$) in the glass adjacent to dissolving crystals of San Carlos olivine, synthetic forsterite, diopside, spinel, quartz and rutile in an andesitic melt. Figures 8–10 include two or more experimental runs of varying duration at the same temperature and pressure. Using normalized distance is a means of comparing profiles produced from differing run duration if the process is strictly diffusion controlled. The profiles are identical within error on such plots when the interface compositions are the same (interface compositions can be used as an internal calibration of run temperature) except for slightly larger uncertainties in the FeO profiles caused by quench magnetites.

It should be noted that many components do not show the expected monotonic concentration profiles but contain "anomalous" minima or maxima (uphill diffusion) in the

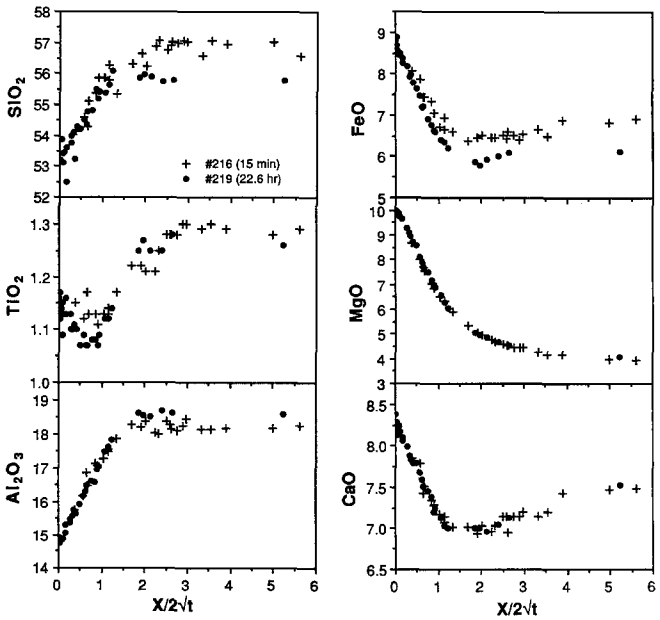

Fig. 8. Concentration profiles for two experiments of olivine dissolution into andesitic melt (# 216 and # 219, T = 1250° C; P = 5.5 kb) vs $x/2\sqrt{t}$. Run duration is in parentheses. The agreement of the concentration profiles suggests that Soret effect is negligible for run duration up to 23 h for # 219 which is the longest of all the experiments

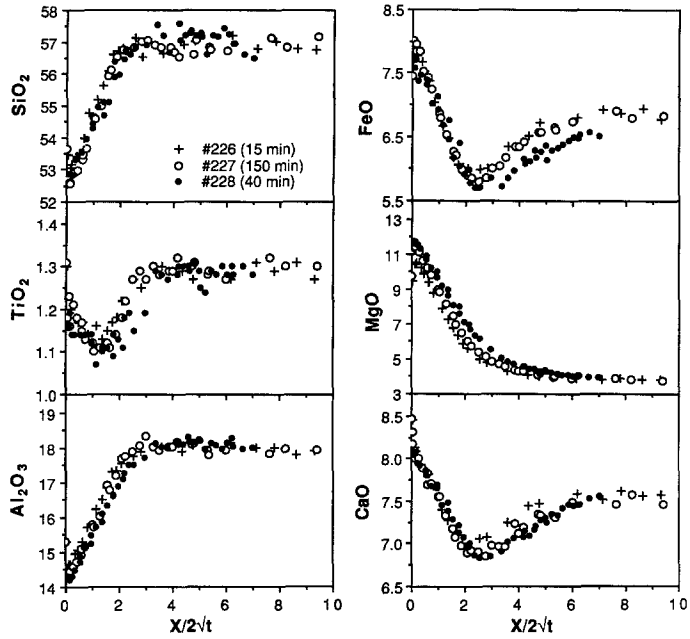

Fig. 9. Concentration profiles for three experiments of forsterite dissolution into andesitic melt (# 226, # 227, and # 228, T = 1285 to 1300° C; P = ~5 kb) vs $x/2\sqrt{t}$

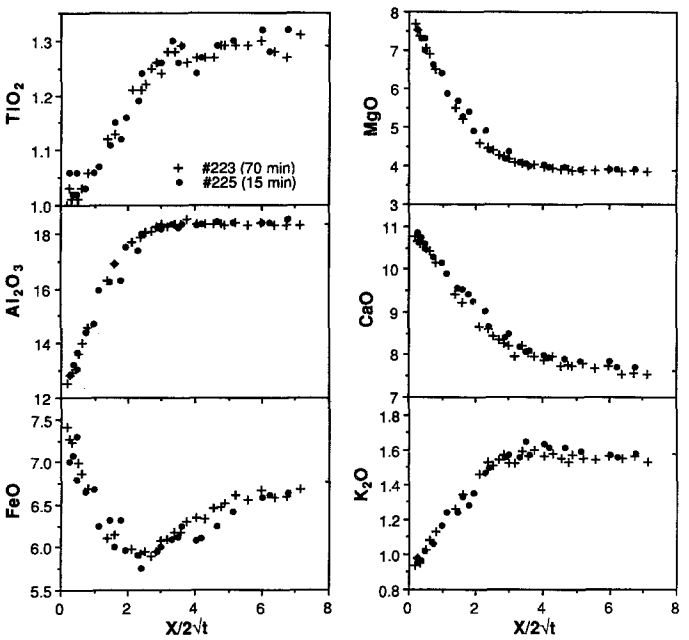

Fig. 10. Concentration profiles for two experiments of diopside dissolution into andesitic melt (# 223 and # 225, T = 1305° C; P = 10.5 kb) vs $x/2\sqrt{t}$

profiles. Concentration profiles for these components on plots using normalized distance are also independent of run duration, which again demonstrates diffusion control. Therefore all the concentration profiles in Figs. 8–10 demonstrate that convection in the melt is not operative and that interface reaction is unimportant.

Uphill diffusion and compositional path

The observed diffusion behavior of major components during diffusive dissolution of various minerals in andesitic melt

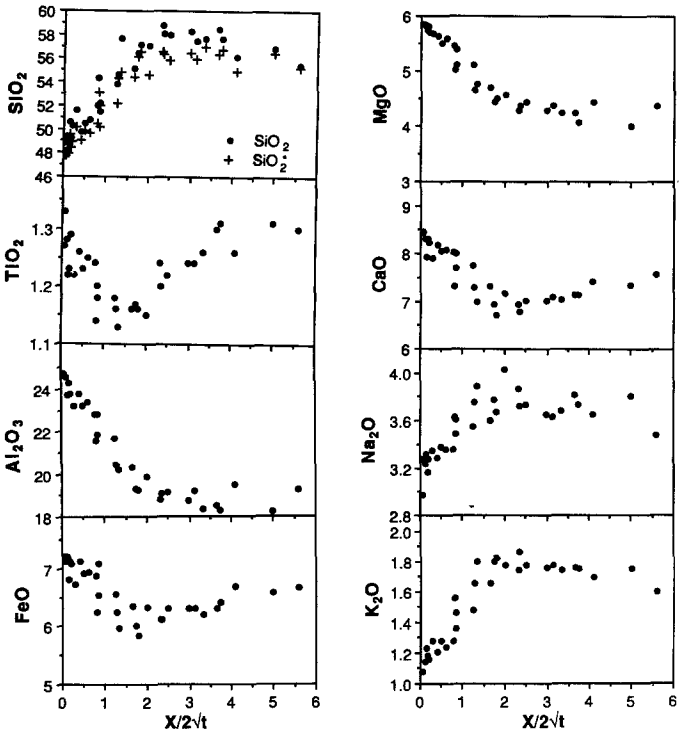

Fig. 11. Concentration profiles for a spinel dissolution experiment in andesitic melt (# 231, T = 1385° C; P = 13 kb) vs $x/2\sqrt{t}$. $SiO_2^* = SiO_2 + 100\text{-Total}$

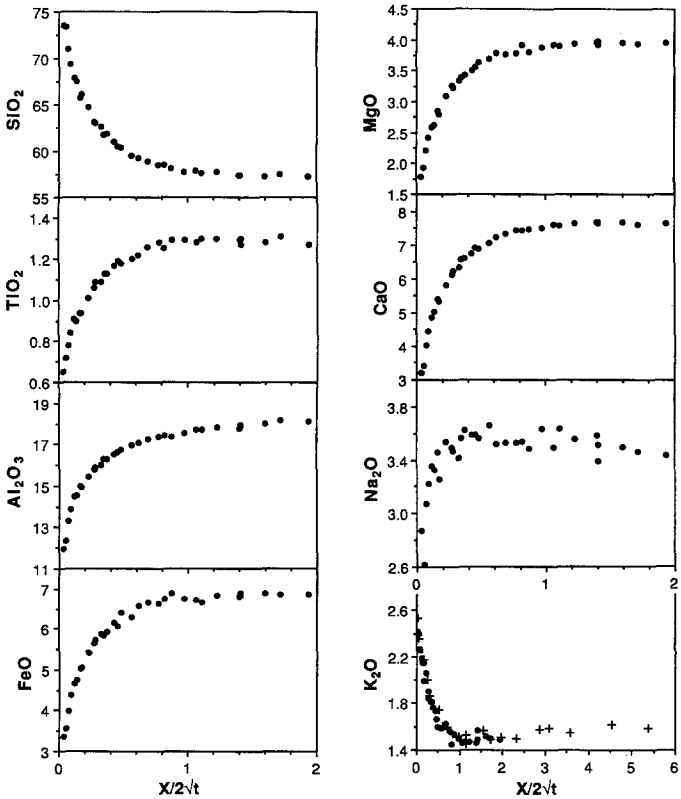

Fig. 12. Concentration profiles for a quartz dissolution experiment in andesitic melt (# 234, T = ~1300° C; P = 5.5 kb) vs $x/2\sqrt{t}$. Notice change in scale for K_2O profile to show the broad minimum at $x/2\sqrt{t} = 1.2$

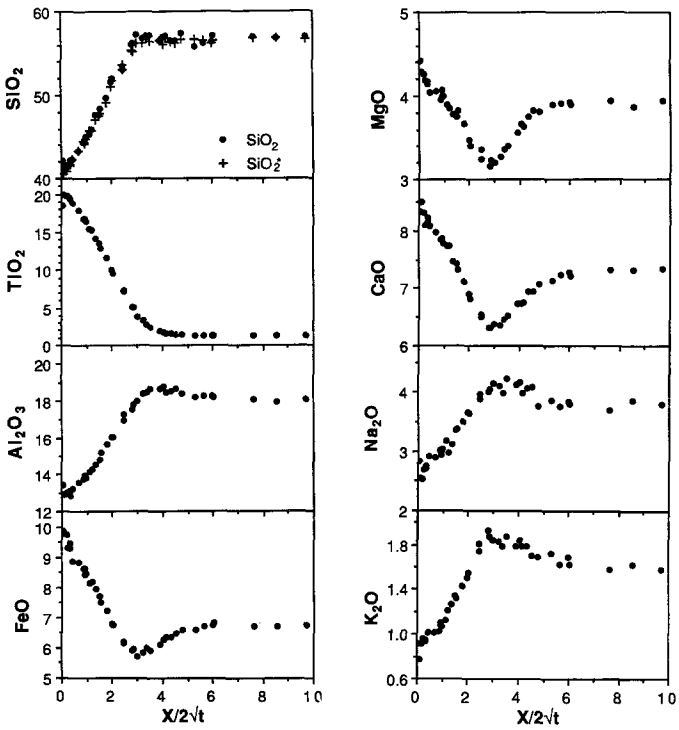

Fig. 13. Concentration profiles for a rutile dissolution experiment in andesitic melt (# 236, T = 1375° C; P = 15 kb) vs $x/2\sqrt{t}$. $SiO_2^* = SiO_2 + 100\text{-Total}$. The interface TiO_2 of ~21% agrees well with the predicted TiO_2 solubility (21.2% at 1375° C and 15 kb with FM = 9.0 for interface melt) using data of Ryerson and Watson (1987)

Table 5. Diffusion behavior of major components during different mineral dissolution

	Oliv	Diop	Spinel	Quartz	Rutile
SiO_2	N	–	N	N	N
TiO_2	UHD(L)	N	UHD(L)	N	N
Al_2O_3	N	N	N	N	UHD(M)[a]
FeO	UHD(L)	UHD(L)	UHD(L)	N	UHD(L)
MgO	N	N	N	N	UHD(L)
CaO	UHD(L)	N	UHD(L)	N	UHD(L)
Na_2O	UHD(M)	–	UHD(M)	–	UHD(M)
K_2O	UHD(M)	UHD(M)	UHD(M)	UHD(M)	UHD(M)
Ref run #	212, 226	223, 242	231	234	236

Note: *N*: Normal diffusion profiles; *UHD(L)*: Uphill diffusion toward less polymerized melt; *UHD(M)*: uphill diffusion toward more polymerized melt; — cannot be determined; [a] weak uphill diffusion toward higher SiO_2 and lower TiO_2, similar to the alkalies

is summarized in Table 5. A surprising observation from this table is the widespread occurrence of "anomalous" diffusion.

During San Carlos olivine and synthetic forsterite dissolution in andesitic melt, only MgO, Al_2O_3, Cr, and SiO_2 show the expected monotonic diffusion profiles (Figs. 7–9). The profiles of alkalies show maxima and those of other major (CaO, FeO, TiO_2) and trace components (V, Sc, Sr, Zr, Y and Ce) show minima. For example, the CaO profiles for the San Carlos olivine and synthetic forsterite dissolution and the FeO profiles for forsterite dissolution have prominent minima in the middle of the profiles. The concentrations of both CaO and FeO increase toward the interface even though the concentrations of these components are low in the dissolving crystals. Barring "anomalous" diffusion, one would expect concentrations to decrease approaching the interface. The anomalous diffusion profiles of these components are indicative of uphill diffusion, i.e. diffusion up their own concentration gradients. The alkalies diffuse uphill toward more polymerized melt (away from the olivine-melt interface) while all other components diffuse uphill toward less polymerized melt.

During diopside dissolution in andesitic melt (Fig. 10), SiO_2 contents are almost constant. MgO, CaO, Al_2O_3 and TiO_2 show "normal" diffusion profiles. FeO diffuses uphill toward the less polymerized melt and the alkalies diffuse uphill toward the more polymerized melt.

During spinel dissolution in andesitic melt (Fig. 11), only SiO_2, Al_2O_3, and MgO show normal diffusion profiles. TiO_2, FeO and CaO diffuse uphill toward less polymerized melt. The alkalies diffuse uphill toward more polymerized melt.

During quartz dissolution in andesitic melt (Fig. 12) only K_2O among all the major components shows strong uphill diffusion toward the more polymerized melt. The Na_2O profile is surprisingly short.

During rutile dissolution in andesitic melt (Fig. 13), only SiO_2 and TiO_2 behave normally. All other major components diffuse uphill. Among them, FeO, MgO and CaO diffuse uphill towards less polymerized melt, and the alkalies and Al_2O_3 diffuse uphill towards more polymerized melt.

Summarizing the above information, we have the following:

(1) During diffusive dissolution of a mineral, the diffusion of various components can be divided into three groups. One is a principal equilibrium-determining component for the dissolving crystal which does not necessarily have to be a major element in silicate melts (such as Zr during zircon dissolution). Another group is the non-participating components, which are only trace constituents of the dissolving mineral. The third group involves the participating but not equilibrium-determining components (such as Si during zircon dissolution). A principal equilibrium-determining component (if there is one) for mineral saturation is expected to behave "normally" and can be approximately characterized as effectively binary. Such components are essential constituents of the dissolving mineral and play the most important role in the saturation of the dissolving mineral. They are: MgO during olivine (Fo # > 50) dissolution; MgO and CaO during diopside dissolution; Al_2O_3 during spinel dissolution; SiO_2 during quartz dissolution and TiO_2 during rutile dissolution. The participating and non-participating elements which include some major elements as well as trace elements can show either "normal" or uphill diffusion.

(2) SiO_2 usually shows normal diffusion profiles.

(3) If uphill diffusion occurs, the alkalies diffuse uphill toward more polymerized melt, while MgO, CaO, Sr, TiO_2, FeO, MnO (by inference to FeO), V, Sc, Y, and Ce diffuse uphill toward less polymerized melt. The uphill diffusion of alkalies toward more polymerized melt is consistent with the reports of Sato (1974), Watson (1982a) and Fisk (1986). FeO enrichment near olivine-melt interface (less polymerized melt) has been noted by Donaldson (1985). However, the result of CaO which diffuses uphill toward a melt of lower SiO_2 during olivine and spinel dissolution differs from the experimental results of Fisk (1986) who found CaO to

be enriched in the higher SiO_2 and lower Al_2O_3 melt formed during the interaction of basaltic melt with a harzburgite. We do not know how to reconcile this difference although we note that Fisk's data showed some scatter and that he did not measure the full concentration profile. Uphill diffusion of other components, including MgO, TiO_2, Sr, V, Sc, Y, and Ce, has not been reported previously, although in theory every component can be made to diffuse up its own concentration gradient (Anderson 1981).

We can conclude from the uphill diffusion behavior of these components that the alkalies partition strongly into more polymerized melt, while most other elements, including MgO, CaO, Sr, TiO_2, FeO, MnO (by inference to FeO), Sc, V, and Ce partition preferentially into a less polymerized melt. These results are consistent with two-liquid partitioning studies (Watson 1976; Ryerson and Hess 1978) and Soret diffusion studies (Lesher 1986). Therefore the diffusion behaviors of non-participating components can be qualitatively predicted using results from two-liquid partitioning or Soret diffusion studies. However, to quantitatively predict their diffusion behavior (such as their interface concentration, where the maxima or minima would occur and what the maxima or minima are), we must await the solution of the full diffusion matrix, including the cross-term coefficients.

Because of the uphill diffusion of certain components and differences in diffusion rates, the melt concentration profiles produced during dissolution are not simple mixtures of initial melts and crystals. In other words, the melt composition does not follow a linear path in composition space between the initial melt and crystal. This non-linearity is evident upon examination of our concentration profiles in Figs. 7–13. It can also be studied using other kinds of diagrams. For example, Fig. 14 is the ol-di-silica ternary projection after Walker et al. (1979). On such a diagram, the minerals being dissolved are conveniently located at the apices, and the compositional effect of adding a mineral is easily seen. The melt composition path during olivine dissolution shown in Fig. 14 is curved and the point of strongest curvature corresponds to the minimum for the CaO profile (Fig. 7a). The melt composition first moves from the initial melt toward a mixture of olivine and silica, and near the interface it moves toward a mixture of olivine and diopside instead of towards a pure olivine composition. Therefore, the melt composition seems to be produced by the addition of more than one mineral even though only one mineral is dissolving. During diopside dissolution, the melt composition path is much less curved and moves roughly towards the diopside apex (Fig. 14). This apparent linearity results from the fact that only one major component, FeO, shows strong uphill diffusion and this one component is grouped together with MgO in calculating the diagram. Thus the non-linearity does not show up strongly in this particular view of composition space. The melt composition path during quartz dissolution is slightly curved but moves roughly toward the silica apex.

Since many components may diffuse uphill, one may conclude that the degree of saturation of the melt, w as defined in (2) and described by (9), could not be described by effective binary diffusion. That is, the effective binary diffusion coefficient defined by (10) would not be approximately constant. However, one should recall that w is mostly determined by the principal equilibrium-determining component, while only affected in a minor way by those components which show uphill diffusion. In other words, k_i for the principal equilibrium-determining component is much greater than k_i for other components in Eq. (6). Figure 15 plots w (see Table 1 for calculation) versus $x/2\sqrt{t}$ for experiment #212. It can be seen that w behaves approximately "normally", similar to the diffusion profile of MgO. The $\bar{D}$ as defined in (10) can be found from the profile in Fig. 15 and determined to be 4.8×10^{-8} cm^2/s, similar to the EBDC of MgO (5.3×10^{-8} cm^2/s, see later discussion on EBDC).

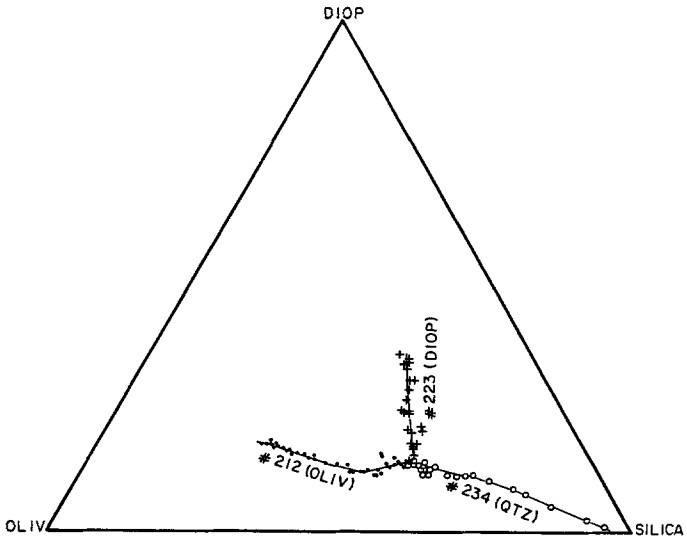

Fig. 14. OL-DI-SILICA triangular plot of composition paths calculated by the Walker et al. (1979) formula during dissolution of olivine, diopside and quartz

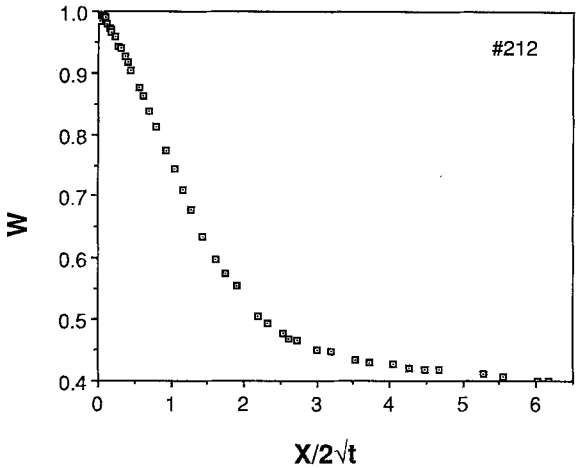

Fig. 15. The degree of saturation (w) vs normalized distance ($x/2\sqrt{t}$). w is calculated from experimental concentration profiles of # 212 (olivine/andesite, 1285° C, 5.5 kb, 5 h). w behaves approximately "normally" despite the fact that many components show uphill diffusion

Discussion and applications

Extraction of EBDC's

Diffusion-controlled dissolution experiments provide a powerful tool for studying the diffusion process. Because the crystal-melt interface is well-defined, distance from the interface can be determined on the electron microprobe to

a precision of 1 μ. The concentration profiles presented in Figs. 8–10 (which plot concentration profiles for two or more runs) show negligible inter-run error using normalized distance $x/2\sqrt{t}$, demonstrating good analytical precision and experimental reproducibility. It is common practice to calculate an effective binary diffusion coefficient (EBDC) for single components in multi-component systems although its applicability is limited. This calculation can be done in a straightforward way using data from diffusive dissolution experiments for any component that does not show uphill diffusion, either by fitting a non-linear least squares curve using Eq. (13) to the concentration profile and thus obtaining one EBDC for each profile, or by using Boltzmann-Matano analysis (Shewmon 1963) to obtain the EBDC as a function of concentration. Equation (13) fits "normal" profiles fairly well but not exactly. For example, as shown by Fig. 16, when MgO diffusion profiles are fit by (13), there are small, but systematic deviations in the data arrays above and below the best fit curves in the higher SiO_2 and lower SiO_2 portions of the MgO concentration profiles. Thus the inherent error in the fit arises more from systematic problems in describing the array by (13) than from scatter in experimental data. If one tries to ascribe these systematic problems to the compositional dependence of the EBDC of MgO (i.e., Boltzmann-Matano analysis) a higher MgO EBDC is extracted for higher SiO_2 melts (i.e., more polymerized melt) – a result which appears intrinsically unreasonable because experimental evidence shows that the diffusivities decrease as the degree of polymerization of the melt increases (Hofmann 1980; Watson 1982a; Lesher and Walker 1986a). Thus, even relatively well-behaved components such as MgO appear to hint in their diffusivities at the complex interdependence of the chemical and diffusion potentials of all the components upon one another's gradients – which is manifested so emphatically in the uphill diffusion phenomenon. (Therefore Boltzmann-Matano analysis is not applicable because the EBDC's, in principle, are not only functions of concentrations of all components, but also functions of the concentration gradients of other components due to cross term diffusion effects.) Nevertheless these errors are small for MgO (total variation of EBDC in a complete profile using Boltzmann-Matano analysis is about a factor of 2, and average EBDC's between different runs agree within 40%; see Fig. 17) and instructive comparative information can be obtained from EBDC's calculated by Eq. (13). However for components which do show uphill diffusion, neither effective binary diffusion with constant EBDC nor Boltzmann-Matano analysis adequately describes their diffusion behaviors. The EBDC's would change from positive to negative using Boltzmann-Matano analysis, which is physically unreasonable. To describe the uphill diffusion phenomenon, multicomponent chemical diffusion must be considered. In principle, this problem is tractable and methods of analysis are available (e.g., Ghiorso 1987). However, in practice, the problem for natural silicate melts (e.g., andesitic liquid) is complicated because at least eight components (SiO_2, TiO_2, Al_2O_3, FeO, MgO, CaO, Na_2O, K_2O) must be considered and thus the diffusion coefficient matrix contains 49 elements. An attempt to invert for these coefficients showed that, although many cross-coefficients were non-zero, they were poorly constrained by the data. In view of the limitations of the present data set we feel it premature to present the results of this analysis here. Additional work is under-

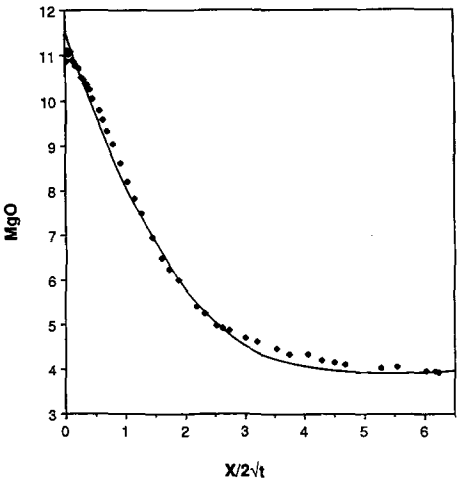

Fig. 16. The best-fit curve of MgO concentration profile using Eq. (13) for experiment # 212. Actual data points are also shown. The equation of the best-fit curve is:
$MgO = 3.95 + 7.82\ \mathrm{erfc}[0.43(x/2\sqrt{t} - 0.23)]$

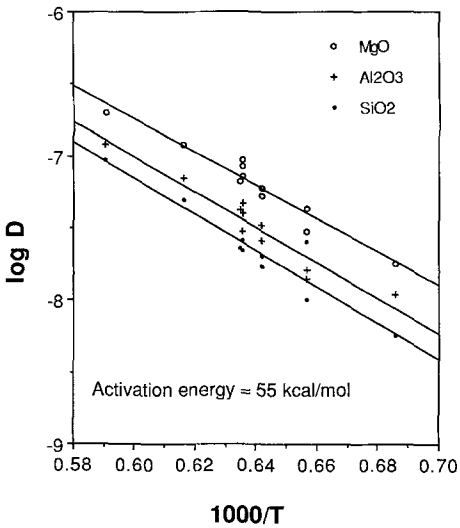

Fig. 17. EBDC (cm^2/s) of SiO_2, Al_2O_3 and MgO for olivine and forsterite dissolution into andesitic melt at 5 kb vs 1000/T in an Arrhenius plot. The temperature is calculated from olivine saturation surface at 1 atm (4th column in Table 3). Best fit straight lines are also shown

way to acquire the experimental data needed for more thorough treatment of multicomponent diffusion in andesite liquid. The results of this more complete treatment will be presented in a subsequent report. However, even with this accomplished, EBDC's still give practical and useful constraints on diffusion distances and dissolution rates in magmatic liquids. Such information has direct applicability to a wide range of immediately relevant petrologic problems. We discuss some of these applications in subsequent sections.

EBDC's obtained from our diffusive crystal dissolution experiments using (13) are listed in Table 6. Uncertainties for EBDC's depend on the analytical error, whether or not the component is well described by effective binary diffusion, how large a portion of the profile in terms of normalized distance is affected by the quench crystal growth, and if

Table 6. EBDC

Run #	D_{MgO}	$D_{Al_2O_3}$	D_{SiO_2}	D_{CaO}
212(OL)[a]	5.3	3.3	2.0	–
216(OL)	4.3	1.4	2.5	–
219(OL)	3.0	1.6	1.0	–
222(OL)	6.6	4.2	2.3	–
223(DI)	4.4	2.5	–	8.6
225(DI)	5.1	3.8	–	9.5
226(FO)	6.0	2.6	1.7	–
227(FO)	7.1	3.0	2.6	–
228(OL)	8.5	4.0	2.2	–
228(FO)	9.4	4.7	2.6	–
229(OL)	1.8	1.1	0.57	–
231(OL)	11.4	8.5	3.6	–
231(SP)	8.5	3.8	2.5	–
231(DI)	10	7.3	–	22
234(QT)	0.2	0.42	0.28	0.21
235(OL)	12	7.0	5.0	–
236(OL)	24	16	12	–
236(RT)[b]	–	–	5.5	–
239(OL)	20	12	9.4	–
242(DI)	18	10	–	26

Note: The EBDC's are for oxide components in μ^2/s. *Run #*: Included in parenthesis is the crystal for which the dissolution distance is measured and near which the profile is considered. Relative errors (at 1σ level) from the curve fitting are small, usually less than 10%. However, a more realistic measure of errors comes from inter-run comparisons and can be estimated from Fig. 17
— the EBDC cannot be calculated because of uphill diffusion or because the concentration is almost constant; [a] Cr diffusion coefficient is 3.6 μ^2/s; [b] TiO_2 diffusion coefficient is 8.2 μ^2/s

Table 7. Dependence of EBDC on the minerals being dissolved

Mineral	D_{SiO_2}	$D_{Al_2O_3}$	D_{MgO}	D_{CaO}	Ref Run #
Andesitic melt at T≈1300° C and P≈5 kb					
Oliv	2.3	4.2	6.6	–	222
Quartz	0.28	0.42	0.20	0.21	234
Andesitic melt at T≈1375° C and P≈13 kb					
Oliv	3.6	8.5	11	–	231
Diop	–	7.3	10	22	231
Spinel	2.5	3.8	8.5	–	231
Andesitic melt at T≈1375° C and P≈15 kb					
Oliv	12	16	24	–	236
Rutile	5.5	–	–	–	236

Note: Unit for EBDC is μ^2/s
Although the nominal temperatures for # 231 and # 236 are similar, the difference in the interface MgO concentrations near olivine crystals suggests that temperature for # 236 is ~40° C higher than for # 231

convection is present. Such uncertainties are difficult to estimate. Nevertheless, based on data scatter in various plots and on other considerations, the relative error for EBDC's is estimated at ±30%.

Dissolution of different minerals not only modifies the chemical composition of the original melt, but also sets up different compositional gradients. Therefore EBDC's are expected to correlate somewhat with the minerals being dissolved. The question is to what extent the EBDC's change with different minerals and whether it is appropriate to use EBDC's extracted from diffusive dissolution experiments of one mineral to predict the diffusive dissolution of another mineral or, in general, to estimate the diffusion in similar melts but different compositional gradients. Table 7 lists 3 groups of EBDC data for comparison. In each group temperature and pressure are similar but the minerals being dissolved are different. With the notable exception of the olivine-quartz group at 1300° C and 5 kb, the EBDC's for different minerals agree with one another within a factor of 2–3, which is only slightly larger than the uncertainties of our EBDC data. The olivine-quartz group is an extreme case in that the SiO_2 content in the melt changes from 52% at the olivine-melt interface to more than 70% at the quartz-melt interface. Diffusivities are expected to change by more than a factor of 10 in that SiO_2 concentration range (Watson 1982a; Lesher and Walker 1986a). Therefore the change in the EBDC can be attributed to a change in chemical composition. For the other two groups, the change in SiO_2 content is much less drastic and that change is often balanced by another potential network-forming component (high SiO_2 by low Al_2O_3 for diopside, low SiO_2 by high Al_2O_3 for spinel, and low SiO_2 by high TiO_2 for rutile). These results suggest that EBDC's depend more on chemical compositions than an compositional gradients for the principal equilibrium-determining components or for the components which behave normally.

The EBDC's of MgO, Al_2O_3, and SiO_2 during San Carlos olivine and synthetic pure forsterite dissolution at 5 kb are plotted in Fig. 17 on an Arrhenius diagram to show the temperature dependence of the EBDC's. The best-fit lines on such a plot for the three components are parallel, implying that the activation energies of the three components are similar, ~55 Kcal/mol, which compares favorably with the results of Lesher and Walker (1986b). The scatter on this diagram can be used to gain some estimate of the magnitude of the relative errors on EBDC's. Figure 18a through 18c are summary plots of EBDC's extracted from all our experiments. The plots indicate little, if any, pressure dependence of EBDC's for MgO, Al_2O_3 and SiO_2 in andesitic melt at 1300°–1400° C.

The EBDC's obtained from this study can be compared with EBDC's obtained in previous studies, although diffusivities in some of these previous works were not extracted correctly and cannot be directly compared (see later discussion). Considering differences in run conditions and melt compositions, the SiO_2 diffusivity during quartz dissolution into andesitic melt determined in this study (2.8×10^{-9} cm^2/s at 1300° C and 5.5 kb) agrees well with that for quartz dissolution into basaltic melt (0.9×10^{-9} cm^2/s at 1300° C and 1 atm for the stirred runs) determined by Watson (1982a), and that extracted from rhyolite-dacite interdiffusion couples (1×10^{-9} cm^2/s at 1300° C and 5 kb) by Baker (1988). Baker's (1988) results are comparable to these for quartz dissolution because the interface melt composition in these latter experiments is rhyolitic. D_{SiO_2} (8×10^{-8} cm^2/s) obtained from Soret diffusion study (Lesher and Walker 1986a) for Mt. Hood andesite at 1475° C (average temperature) and 10 kb agrees within a factor of 2 with that extrapolated from this study (1.7×10^{-7} cm^2/s) for olivine dissolution into andesitic melt at 1475° C and 5 kb). The limited data seem to suggest that the EBDC's obtained from diffusive crystal dissolution are not only internally consistent, but also comparable with those obtained by other methods at similar conditions. Therefore we can apply

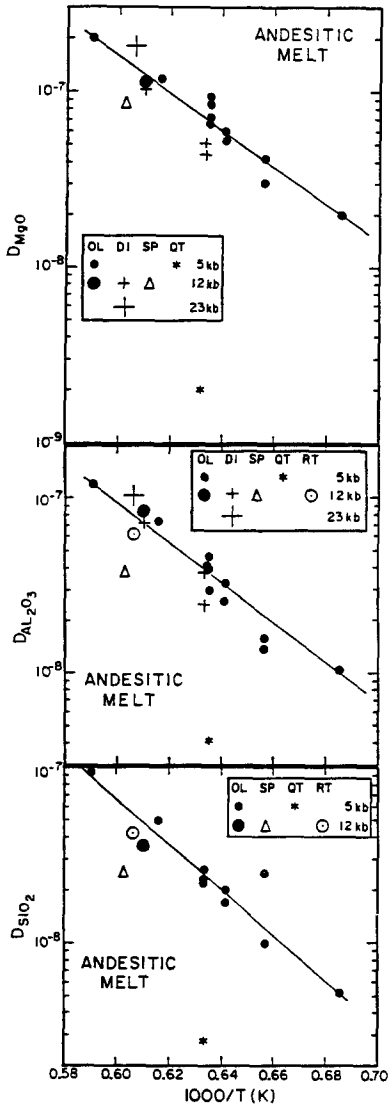

Fig. 18. EBDC (cm^2/s) of SiO_2, Al_2O_3 and MgO for all experiments. The temperature is the calculated temperature (4th column of Table 3) for ~5 kb runs with olivine crystal and the nominal temperature (2nd column of Table 3) for all other runs

EBDC's extracted from diffusive dissolution studies to other general diffusion problems of systems of similar compositions.

Caveat on extracting EBDC's

There is considerable confusion in the literature over extracting EBDC's from dissolution experiments. Some authors (Brearley and Scarfe 1986, and Kuo and Kirkpatrick 1983) have tried to extract EBDC's from steady-state diffusion profiles during crystal dissolution in which they recognized that the steady-state was caused by free convection. The following equation was used to extract EBDC's:

$$\frac{C_l}{C_i}=1+\left(\frac{1-k}{k}\right)e^{-ux/D} \tag{17}$$

where the subscript l refers to the liquid and i refers to the initial liquid, k is the distribution coefficient between crystal and melt, and u is assumed to be the steady-state *dissolution* rate. There are several difficulties with the application of (17) to crystal dissolution data. The first is that (17) represents the solution for steady-state, non-convective, constant-rate crystal *growth* where u should be the constant crystal *growth* rate. When the same equation is used for crystal dissolution, u must be taken as the negative of dissolution rate. As such Eq. (17) does not approach a constant value when the concentration profile does at large x; therefore (17) is not an appropriate solution for describing steady-state diffusive dissolution. This conclusion reflects the impossibility of developing a steady state during strictly diffusive dissolution except in the trivial case of constant C_l. This impossibility is a fundamentally different characteristic of the dissolution as opposed to the crystallization process. In crystallization, a steady state can be reached eventually through the operation of interface equilibrium as the crystal forms. The crystal "finds" the appropriate solute level (unless saturation effects intervene), which is the same as the melt far away (Albarede and Bottinga 1972; Lasaga 1981). Diffusion and interface motion respond by partitioning the solute between crystal and melt, to produce a steady state. However in dissolution, the arbitrary choice of disequilibrium crystal composition insures that no steady state will develop. The applicability of (17) is limited at best.

Experimentally, however, steady states are observed to form during crystal dissolution when free convection is possible in addition to diffusion. The difficulty with applying (17) in such situations is that u can no longer be directly associated with the rate of change of crystal size measurements. The u which makes (17) a viable description of diffusive-advective dissolution data must be positive. Because the dissolution rate alone used in (17) is negative, it cannot be u. However, the advection rate associated with free convection can be positive and larger than the dissolution rate. Adding the rates of dissolution and advection, the right side of (17) can converge to a constant value at large x and describe a steady state. But the u of interest – an amalgam of the dissolution and advection rates – is no longer physically measurable. What is measurable is the slope of the plot of $\log[(C_l-C_i)/(C_0-C_i)]$ versus x. This slope will be $-u/D$ where u is the composite of diffusion and advection rates. But until u can be calculated from its component rates (only the dissolution rate being directly measurable), D cannot be properly extracted from the data by (17). Using the measured dissolution rate instead of u will probably give values of D that are too small (of the wrong sign), because

$$\text{true } D=\frac{\text{Dissolution rate}+\text{Advection rate}}{(u/D)}$$
$$>\frac{\text{Dissolution rate}}{\text{observed slope}}<0. \tag{18}$$

D/u has the dimensions of length and can be regarded as a scale thickness for the diffusive boundary layer between the dissolving crystal and the homogeneous, well stirred, distant liquid. Low chemical diffusivity can keep the chemical boundary layer profile (D/u) adjacent to a dissolving crystal thin, but so can advection by increasing u. Equation (18) shows that apparent EBDC's extracted from observations of the dissolution rate and the boundary layer thickness (D/u) using Eq. (17) will be unrealistically low.

For a particular liquid composition, the diffusivity of a given component at fixed P, T should be constant. Brear-

ley and Scarfe (1986) noted the nonconstancy of their EBDC's in a particular alkali basalt at one P, T: "The apparent diffusivities positively correlate with the dissolution rate, which suggests that the stability of the mineral is an important factor to consider when deriving diffusion coefficients from these experiments." (Brearley and Scarfe 1986, in the abstract). Part of this problematic observation can probably be traced to the questionable application of Eq. (17). The EBDC's were probably extracted by multiplying the value D/u gained from analysis of the data using (17) by the dissolution rate. Because D/u varied little in their experiments, their EBDC's were forced to correlate with the dissolution rates. In our strictly diffusion-controlled experiments (where we do not use [17] in the analysis), we see quite subdued variations of EBDC's at one P, T compared to those of up to a factor of 36 found with inappropriate use of (17) in advection-diffusion of spinel and diopside dissolution experiments. Of course, we cannot confirm that this large variation in EBDC's is an artifact of the calculation process, because it is not possible to accurately extract the EBDC's from advection-diffusion experiments by (17).

We do not wish to imply that there should be no variation in the EBDC's at one P, T. It is reasonable to expect EBDC variations to correlate with dissolution rate, because the dissolution rates are controlled to some extent by the diffusivities. In fact, we do see nontrivial variations in the EBDC's at one P, T in our data. The question is how does this happen in, for instance, a single andesite melt? The EBDC variations in our experiments arise because the melt through which the MgO, for example, diffuses is not of identical composition during the dissolution of each of the different minerals, even though the melt at some distance is the same in each case. Furthermore the concentration gradients adjacent to the crystals during the dissolution of different crystals are variable. The variations of EBDC's have nothing directly to do with the mineral stabilities or interface reaction kinetics (for example, the slow dissolution rates of zircon and apatite in silicate melts are due to their solubilities, the diffusivities will not be proportionally reduced by the slow dissolution rates). Melt EBDC's do not depend on mineral properties but on those of the liquid. The apparent dependence of EBDC on the mineral being dissolved is indirect, due to controls on the chemistry of the melt adjacent to the crystal.

Convective dissolution rate

The following approximate method may be utilized for analyzing dissolution and diffusion in a convective regime as steady-state is reached. The diffusion in such a convective regime can be characterized as occurring across a steady-state boundary layer which, in turn, is characterized by a boundary layer thickness (δ). Although this boundary layer thickness does not vary with time (definition of steady-state), it may vary from place to place due to convection patterns. In this case, the average is used to characterize the boundary layer. Because the motion of melt relative to the crystal decreases gradually to zero at the interface, the only mechanism of mass transport at the interface is diffusion (Lasaga 1981). Therefore Eq. (12e) is always applicable at the interface. According to the definition of δ:

$$\delta=(C_\infty-C_0)/(\partial C/\partial x)_{x=0} \tag{19}$$

Combining (19) and (12e), we have

$$V=\frac{D}{\delta}\frac{C_0-C_\infty}{C_s-C_0}=b\frac{D}{\delta} \tag{20}$$

Parameter b in (20) is defined in (14b). The above equation is similar to Eq. (13) of Kuo and Kirkpatrick (1985), and it applies also to diffusive dissolution if δ is viewed as the time-dependent diffusion layer thickness. The convective dissolution rate is therefore a function of initial melt and crystal compositions, interface melt composition, the EBDC, and the boundary layer thickness. Applying (20) we can estimate the diffusivities of a component or dissolution rate of a crystal in a given natural or laboratory system, for instance, in the results of Brearley and Scarfe (1986). D can be calculated with known δ (calculated from concentration profiles) and V. The D thus calculated differs from that of Brearley and Scarfe (1986) by a factor of $1/b$ which is likely to be greater than 1 for their experiments, and to be different for different minerals. With known D, V, and δ, even the advection rate $(u-V)$ can be estimated using (17). This kind of exercise may not provide accurate EBDC's and advection rates, however, because boundary layer thicknesses vary and concentration profiles are likely to be nonsymmetric (for the spherical case) or horizontally heterogeneous (for the one-dimensional case). From Eq. (17) the convective dissolution rate is proportional to the parameter b rather than the parameter a of diffusive dissolution. But this does not affect our discussion about relative dissolution rates from an earlier section because b is positively correlated to a, as long as the boundary layer thickness during the dissolution of different minerals is similar. Kuo and Kirkpatrick (1985) observed higher dissolution rates for diopside than those for forsterite, which is consistent with our conclusion. Brearley and Scarfe (1986) observed that cpx dissolves faster than olivine at low pressure and spinel dissolves slower than olivine and pyroxenes. They also found that at higher pressures where cpx is the liquidus phase, cpx dissolves slower than olivine when experimental temperature is only slightly higher than the liquidus, and faster than olivine when experimental temperature is significantly higher than the liquidus temperature. These results are all consistent with our predictions if the full Eq. (20) is used because at temperatures close to the liquidus, the interface melt near cpx is similar to the initial melt composition, which results in a lower dissolution rate for the liquidus phase (cpx).

Estimate of interface composition and predictability of the dissolution rates

Diffusive dissolution distances can be calculated by (12b) from the EBDC of a well-behaved component and the parameter a which depends on the initial crystal and melt compositions and the interface melt compositions. Dissolution distances thus obtained are compared with observed dissolution distances (or those calculated from mass balance) in Table 4. The good agreement between them illustrates the applicability of the formula. Convective dissolution rates given by (20) depend also on the EBDC, initial melt and crystal compositions and interface melt compositions, as well as the boundary layer thicknesses. Therefore, the interface compositions are important parameters in estimating diffusive and convective dissolution rates.

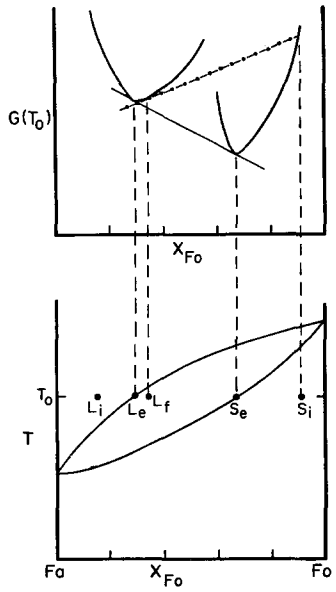

Fig. 19. A sketch phase diagram and Gibbs free energy vs composition for a binary solid solution system showing metastable equilibrium. Starting crystal and melt compositions are S_i and L_i. Equilibrium crystal and melt compositions are S_e and L_e. Possible interface melt composition is between the equilibrium composition L_e and the metastable saturation composition L_f

We have shown that the degree of "saturation" at the interface is essentially 1 after an initiation period of less than a second. One would expect, then, that the interface composition could be predicted from phase equilibria. This is indeed the case for rutile (which is a pure stoichiometric mineral) dissolution where the interface TiO_2 concentration of 20.8% (from second order polynomial fitting of TiO_2 profile of # 236, Fig. 19) agrees very well with the predicted 21.2% using the data of Ryerson and Watson (1987). However, the Fe–Mg exchange coefficient K_D calculated from measured compositions of olivine and the interface melt is about 0.2 during San Carlos olivine dissolution and about 0.01 during dissolution of synthetic pure forsterite. Because equilibrium K_D's are about 0.3 ± 0.03 (Roeder and Emslie 1970), the initial crystal is not in equilibrium with the interface melt for olivine dissolution. This discrepancy can be explained by two possibilities. One is that true local equilibrium may have been achieved between interface crystal and interface melt compositions. Microprobe analysis may not have sufficient resolution to reveal this interface crystal layer, which the slowness of diffusion in a crystal insures will be very thin (furthermore, quench overgrowth complicates the resolution of the thin interface layer). A second possibility, granting the compositional quasi-immutability of the crystal on the dissolution time scale, is that the crystal cannot be in stable equilibrium with the melt given the arbitrary choice of the dissolving crystal (which is a solid solution). For example, consider the Fa–Fo binary system shown in Fig. 19. The dissolving crystal, S_i, can never be in equilibrium with the melt at T_0 or any other lower temperature. The equilibrium crystal will be S_e. (The run temperature is chosen to be lower than the solidus of the crystal in order to avoid internal decomposition.) The free energy surface for liquid and solid solutions are shown schematically in upper diagram of Fig. 19. Because G for crystal S_i is fixed at T_0 due to the lack of compositional exchange, juxtaposition of S_i and melt at T_0 will lead to accommodation of their coexistence via a metastable equilibrium[3], as suggested by the dashed-dot curve on the $G-x$ diagram. Therefore, in this case the interface composition approaches the metastable equilibrium melt L_f rather than the equilibrium melt L_e at T_0. The metastable melt L_f has a higher liquidus, or higher MgO, than the stable equilibrium melt L_e. Nevertheless, we expect $K_D < 0.3$ in this case because the starting crystal composition S_i is even farther from the equilibrium crystal S_e than the metastable melt L_f is from the stable equilibrium melt L_e (Fig. 19). (Note that this kind of metastable equilibrium situation will not happen if the dissolving mineral is a pure stoichiometric mineral, such as rutile, quartz, or zircon.)

To choose between the case of true local equilibrium or metastable equilibrium, an experiment (# 222) was run in which an olivine crystal was centered in the graphite heater with about 50 μ of rock powder on one side and an "infinite" reservoir on the other side. The melt on the thin side should approach the equilibrium composition (assuming the small liquid mass becomes easily saturated) and can be compared to the interface melt on the "infinite" reservoir side. The interface melt on the "infinite" side was found to have higher MgO and FeO and thus had a higher saturation temperature by about 17° C. That is, the interface melt was oversaturated with respect to the equilibrium melt at T_0, as predicted for metastable equilibrium. (The higher FeO is due to uphill diffusion.) Therefore, the interface melt composition is not at equilibrium saturation but rather at a metastable saturation. However, our experiment cannot distinguish whether the interface melt composition is precisely at L_f or at some other metastable composition between L_e and L_f. The metastability of the interface melt suggests that crystal-melt interface equilibrium is not established instantaneously as the melt and crystal come into contact. It also makes precise prediction of interface melt composition impossible, even if phase equilibria are known, though the error due to this may be small.

The second impediment to predicting the interface melt composition is the complicated diffusion behavior of a multi-component system. The composition of the melt does not move along linear paths between initial melt and crystal compositions in composition space as dissolution proceeds (Fig. 14). If it did, interface compositions could be predicted from known phase diagrams as the intersection of the straight line composition path and the liquidus surface of the melt in composition-temperature space, ignoring the small oversaturation. This point is illustrated by the ternary system Ab–An–Di in Fig. 20 (ignoring any non-ternary behavior). During anorthite dissolution in an initial melt A at 1300° C, the interface melt composition after the initiation period should be B (or a little oversaturated with respect to B) if the composition paths were linear. Unfortunately this is not the case. The possible interface melt composition may be somewhere within region C because Na diffuses away from the low-Si interface. Therefore, even if phase equilibria are known, and even if the interface melt composition is near saturation (ignoring the small oversaturation), the interface composition still cannot be evaluated

[3] We call it metastable equilibrium because it represents a local minimum of the Gibbs free energy at the interface. Because the only component that can be exchanged in this case is S_i, only the chemical potential for this component in the two phases needs to be equal at this metastable equilibrium

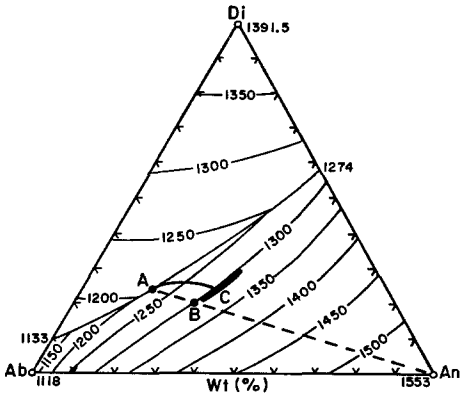

Fig. 20. A ternary phase diagram Di–Ab–An showing the effect of multi-component diffusion. The diagram is adapted from Morse (1980) after Bowen (1915) with revision by Schairer and Yoder (1960), Osborn and Tait (1952) and Kushiro (1973). When anorthite crystals are dissolving in liquid *A* at 1300° C, the interface melt is found at *C* rather than *B* because of uphill and differential rate of diffusion

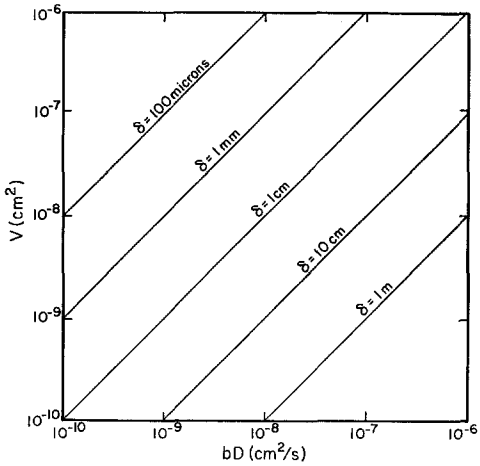

Fig. 21. Calculated dissolution rate vs diffusion coefficient during convective dissolution for a range of boundary layer thicknesses

in a multi-component system without knowing the diffusion coefficient matrix.

Therefore, we conclude that the interface melt composition need not be in stable equilibrium with the *initial* crystal composition (even in a binary system), nor is it predictable for all the components in a multi-component system. Having belabored all this, is it still possible to approximate the stationary interface melt concentrations of some components so that dissolution rate can be estimated? (After all, our mathematical analysis in previous sections demonstrated that a stationary composition should be reached quickly and the interface melt concentration of only one component is enough to estimate the dissolution rate.) The answer is yes because there is usually one component that plays a determining role in the stability of a crystalline phase in a multi-component system. Such a component may have small opportunity for compositional variation because isopleths for this component usually approximate liquidus isotherms in composition space. For instance, An and Di saturation isotherms are nearly An and Di isopleths respectively in Fig. 20. Thus An interface concentration during An dissolution at 1300° C can be roughly estimated to be at 30–36%. Another example is MgO interface concentration during dissolution of olivine. Following Roeder and Emslie (1970) and Langmuir and Hanson (1981), olivine saturation in basaltic melt can be described as:

$$K_d^{MgO}(MgO + K_D\, FeO) = 66.67$$

where MgO and FeO are in cation mole percent, K_D is almost constant (0.3) and K_d^{MgO} is a function of temperature and pressure. Other components have little effect upon olivine saturation. Therefore given the temperature (and pressure), the whole term inside the brackets can be evaluated as $66.67/K_d^{MgO}$. FeO does not affect olivine saturation as much as MgO does. 1% FeO is equivalent to only 0.3 mole% MgO (0.17 wt%) in determining the saturation of olivine. Therefore, with FeO poorly estimated (from initial melt and crystal compositions) we can still estimate interface MgO with reasonable precision. At 1300° C, if interface FeO is about 6–9 mole% (or 8–12 wt%), interface MgO will be 15.8–16.7 mole% (or 11.5–12.2 wt%). Interface MgO concentration during olivine dissolution can be better estimated than interface anorthite concentration during pure anorthite dissolution. In general, the more important the component is in determining the saturation surface of the dissolving crystal, the better the estimate of the interface concentration for the component (for example, TiO_2 concentration at the interface can be estimated fairly well during rutile dissolution). Therefore we can estimate the dissolution rate and dissolution distance during diffusive crystal dissolution using (12b) and phase saturation data. Data on the saturation surfaces of many crystalline phases at different pressures are needed not only for the understanding of crystallization sequences (equilibrium processes), but also for predicting dissolution rates (kinetic processes).

Convective dissolution and magma contamination

During convective dissolution, the least determined parameter involved in estimating dissolution rates by (20) is the boundary layer thickness δ, which is not only difficult to determine but may also vary considerably from place to place near the same dissolution interface. Using δ as a parameter, the dissolution rate V can be plotted against bD (Fig. 21). The thickness must be determined independently in order to estimate the convective dissolution rate. Better understanding of the convection regime about a dissolving crystal (or aggregate in the case of xenolith digestion) or at the reactive margins of a magma chamber is required. Clark et al. (1987) estimated a typical compositional boundary layer thickness of 20 cm adjacent to the wall of a magma chamber. If so, for $D = 10^{-7}$–10^{-8} cm^2/s for basaltic melt and $b = 0.1$–0.3, the dissolution rate in a magma chamber digesting crustal rocks is 0.0015 to 0.05 cm/year. These estimates are much lower than experimentally determined convective dissolution rates (Kuo and Kirkpatrick 1983; Brearley and Scarfe 1986) due to a thicker boundary layer. Dissolution of 10 m of crustal rocks requires 20000–700000 years. Such low dissolution rates would rarely produce significant contamination of magmas with mass diffusivities less than 10^{-7} cm^2/s. Mass diffusivities for komatiitic melts are likely to be 100 times greater due to higher temperature and lower silica content of these magmas. Moreover, boundary layer thicknesses adjacent to conduit walls or surface channels

would be 100 times smaller due to vigorous convection accompanying turbulent flow. These two factors will make dissolution rates ten thousand times faster for these magmas. For example, the erosion of a decimeter deep channel in the continental crust by a continuous komatiite flow would take 0.02–0.7 years. However, this erosion rate is much lower than the thermal erosion rate of 7 m/day suggested by Huppert and Spark (1985) who considered the melting (instead of dissolution) of the wall rock controlled by heat transfer.

Because a continuous heat supply is necessary for a magma body to remain a liquid at its boundaries (so that it can dissolve wall rocks or xenoliths), the most likely situations for rock dissolution are for xenoliths engulfed by the magma and in conduits through which the magma is ascending. The contamination ratio (ratio of the volume of the dissolved wall rock or xenolith to the melt parcel) can be written in the following general form:

$$A^* V t/U$$

where A is the total surface area of the wall rock or xenoliths in contact with the melt, V is the dissolution rate, t is the time scale for dissolution and U is the total volume of the melt. Large xenoliths are not efficient in contaminating the melt both because they do not remain in the magma for long, unless neutrally buoyant, and because of the small A/U ratio. Using an analysis similar to that of Walker and Kiefer (1985), xenolith digestion through crystal dissolution only is not an effective process for contaminating magma, except in the stagnant local region near a xenolith. Digestion of many small (e.g. centimeter size or smaller) xenoliths will be a more effective contamination mechanism if a physical mechanism of xenotlith comminution and dispersal operates (such as melting of the xenolith at grain boundaries if its temperature can be raised high enough). Such a process is limited only by the thermal budget of the magma body.

Interpretation of least squares analysis

The common occurrence of uphill diffusion during diffusive crystal dissolution suggests that the mineral proportions discovered by least squares analyses of complementary liquid fractions may be misleading if diffusion is involved in melt genesis. The melt gains extra components of compositional variability through diffusive separation, in addition to the linear mixing of the actual mineral into the melt. For example, we have tried to reproduce the melt compositional variation in olivine dissolution run # 212 (initial melt is andesitic) by seeking linear combinations of common minerals with the initial melt (Fig. 22). Nontrivial amounts of clinopyroxene, orthopyroxene, and plagioclase in addition to olivine are required to reproduce the melt compositional variations which are generated by diffusive olivine dissolution alone. An almost constant cpx to olivine ratio of about 1–2 would be required. The abundances of some trace elements in the melt (# 212), such as high Sc, V, Y (due to uphill diffusion) and high Cr (due to high Cr in olivine), are also mysteriously consistent with, or apparently require, an addition of high-Ca pyroxene. Of course, in this case we know that other minerals are not physically involved, but diffusion kinetics is. Uphill diffusion can occur during crystal growth as well as during crystal dissolution, although the two processes do not strictly mirror one another. One way in which they differ is that crystal composition responds to the melt composition during crystal growth, but not during crystal dissolution. Thus, the exact characteristics of the uphill diffusion effects during residual melt petrogenesis accompanying crystal growth are difficult to predict from our dissolution experiments, which simply highlight the need to be aware of such complications. When examining compositional variations in natural glasses, one does not know which minerals are involved in the fractionation. Those are usually what one seeks to discover by least squares analyses. If diffusion kinetics are involved, then a least squares analysis may not give either realistic mineral assemblages or the right mineral proportions involved in melt genesis. For example, the residual melt (glass) sampled in an oceanic gabbro may not be simply related to bulk magma composition by least squares analysis of removing crystallizing minerals.

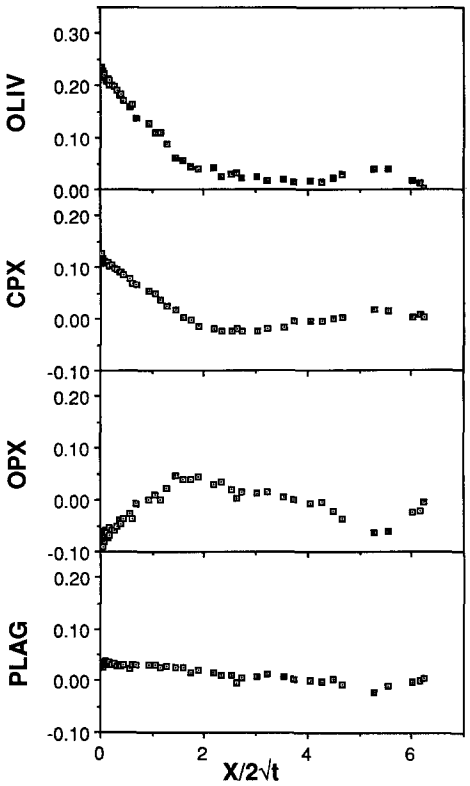

Fig. 22. Hypothetical fraction of oliv, cpx, opx, plag necessary to reproduce melt composition in the diffusion boundary layer produced by olivine dissolution alone (# 212), plotted against $x/2\sqrt{t}$ (in $\mu/\sqrt{s}$). Composition of the minerals used in the least squares analysis: Mg # 80 for mafic minerals and An85 for plagioclase. If Mg # 90 is used, the least squares fit is much less satisfactory (especially for FeO) and even higher ratios of other minerals to olivine are found

The observed diffusion profiles also have ramifications for the study of crystal zonation and for cumulate rocks. Most importantly, the *bulk* magma composition may not be inferred from the zoned crystal or crystal assemblage without a full understanding of the diffusion behavior in a multi-component silicate melt system, if diffusion played some role in the processes.

Conclusions

We studied two of the three basic component parts of the dissolution process: reaction at the crystal-melt interface

and diffusion into the melt. The role of interface reaction has been evaluated numerically and has been found to be relatively unimportant in controlling crystal dissolution rates in silicate melts. Interface kinetics are important only when dissolution temperatures are close to the liquidus of the dissolving crystal, during which it is difficult for the interface composition to reach the stationary "saturation" composition. In most cases crystal dissolution is diffusion-controlled when there is no convection; and is controlled by diffusion across the boundary layer when there is convection. We have also shown experimentally that the concentration profiles of the chemical components during crystal dissolution propagate into the melt according to, and the dissolution distance increases with, the square root of run duration. This documents control by diffusion. Diffusive dissolution can be mathematically analyzed and diffusive dissolution rates can be estimated using saturation conditions and the EBDC of a principal equilibrium-determining component.

Our dissolution results can be applied by extrapolation to natural magmatic systems if convection and other possible complications (e.g., more complex geometry) can be adequately addressed. Convective dissolution rates can be predicted if we know the boundary layer thickness, as well as the EBDC, the initial melt and crystal compositions, and the interface melt compositions. It is found that dissolution alone may not be sufficient to alter magma compositions except during the percolation of melt through wall rocks, if convective compositional boundary layer thickness around ascending magma is 20 cm or greater. Wall-rock dissolution is likely to be subordinate to melting during the crustal contamination of a mantle-derived magma.

Our experiments also provide a method for study of the complicated diffusion process. Our data show that uphill diffusion is the rule rather than the exception, especially during olivine dissolution. Therefore, caution is necessary in modelling trace element zonation in phenocrysts, and in interpreting least squares mass balance analysis, because diffusion may be involved. Solution of the full diffusion matrix of natural silicate melts is required to rigorously model these processes in detail, but much qualitative insight into chemical diffusion in magmas is provided by direct study of mineral dissolution and treatment of experimental data as presented here.

Acknowledgement. This work has benefited from discussions with Drs. N. Shimizu, and D. Christie. Thanks are due to N. Shimizu who did the ion microprobe analysis, Sandy Bromble who helped in electron microprobe analysis, and Peter McNutt for technical assistance. Drs. G. Harlow and T.J. Shankland provided some crystals used in this study. Drs. E.B. Watson and J. Ryan are thanked for their insightful and constructive reviews. Questions raised by Drs. M. Ghiorso, C. Langmuir, G. Muncill, E.M. Stolper and C. Zhu helped clarifying some of the concepts. Daily interactions with Lamont students and research staff contributed in many ways to this manuscript. C. Straub helped in typing the paper. Patty Catanzaro helped in drafting the diagrams. This work is supported by NSF (Grant OCE85-11017, EAR85-13693, and EAR87-07536) and DOE (Grant DE-FG02-84ER13287). Lamont-Doherty Geological Observatory Contribution No. 4484.

References

Albarede F, Bottinga Y (1972) Kinetic disequilibrium in trace element partitioning between phenocrysts and host lava. Geochim Cosmochim Acta 36:141–156

Anderson DE (1981) Diffusion in electrolyte mixtures. In: Lasaga AC, Kirkpatrick RJ (eds) Reviews in Mineralogy 8:211–260 Washington, DC, Mineral Soc Am

Baker DR (1988) Chemical diffusion in intermediate to silicic melts: effects of pressure and fluoridation. EOS 69:511

Bender JF, Hodges FN, Bence AE (1978) Petrogenesis of basalts from the project FAMOUS area: experimental study from 0 to 15 kbars. Earth Planet Sci Lett 41:277–302

Bowen NL (1915) The crystallization of haplobasaltic, haplodioritic and related magmas. Am J Sci (4th Ser) 40:161–185

Brearley M, Scarfe CM (1986) Dissolution rates of upper mantle minerals in an alkali basalt melt at high pressure: an experimental study and implication for ultramafic xenolith survival. J Petrol 27:1157–1182

Clark S, Spera FJ, Yuen DA (1987) Steady state double-diffusive convection in magma chambers heated from below. In: Mysen BO (ed) Magmatic processes: physiochemical principles (Yoder Volume). University Park, Geochem Soc Spec Publ 1:289–305

Cooper AR (1968) The use and limitations of the concept of an effective binary diffusion coefficient for multi-component diffusion. In: Wachtman JB Jr, Franklin AD (eds) Mass transport in oxides. Nat Bur Stand Spec Publ 296:79–84

Cooper AR Jr (1974) Vector space treatment of multicomponent diffusion. In: Hofmann AW, Giletti BJ, Yoder HS Jr, Yund RA (eds) Geochemical transport and kinetics. Carnegie Inst Washington Publ 634, pp 15–30

Crank J (1975) The mathematics of diffusion. Oxford Univ Press, Oxford, pp 414

Denbigh K (1966) The principles of chemical equilibrium. Cambridge Univ Press, Cambridge, p 494

Donaldson CH (1985) The dissolution rate of olivine, plagioclase, and quartz in a basaltic melt. Mineral Mag 49:683–693

Dowty E (1980) Crystal growth and nucleation theory and the numerical simulation of igneous crystallization. In: Hargraves RB (ed) Physics of magmatic processes. Princeton University Press, New Jersey, pp 419–486

Fisk MR (1986) Basalt magma interaction with harzburgite and the formation of high-magnesium andesites. Geophys Res Lett 13:467–670

Ford CE, Russell DG, Craven JA, Fisk MR (1983) Olivine-liquid equilibria: temperature, pressure and composition dependence of the crystal/liquid cation partition coefficients for Mg, Fe^{2+}, Ca and Mn. J Petrol 24:256–265

Ghiorso MS (1987) Chemical mass transfer in magmatic processes. III. Crystal growth, chemical diffusion and thermal diffusion in multicomponent silicate melts. Contrib Mineral Petrol 96:291–313

Harrison TM, Watson EB (1983) Kinetics of zircon dissolution and zirconium diffusion in granitic melts of variable water content. Contrib Mineral Petrol 84:66–72

Harrison TM, Watson EB (1984) The behavior of apatite during crustal anatexis: equilibrium and kinetic considerations. Geochim Cosmochim Acta 48:1467–1477

Hofmann AW (1980) Diffusion in natural silicate melts: a critical review. In: Hargraves RB (ed) Physics of magmatic processes. Princeton University Press, New Jersey, pp 385–418

Huppert HE, Sparks RSJ, Turner JS, Arndt NT (1984) Emplacement and cooling of komatiite lavas. Nature 309:19–22

Huppert HE, Sparks RSJ (1985) Komatiites, I. eruption and flow. J Petrol 26:694–725

Kirkpatrick RJ (1975) Crystal growth from the melt: a review. Am Mineral 60:798–814

Kirkpatrick RJ (1981) Kinetics of crystallization of igneous rocks. Lasaga AC, Kirkpatrick RJ (eds) Reviews of Mineralogy 8:321–389 Washington, DC, Mineral Soc Am

Kuo L-C, Kirkpatrick RJ (1985) Kinetics of crystal dissolution in the system diopside-forsterite-silica. Am J Sci 285:51–90

Kushiro I (1973) The system anorthite-diopside-albite: determination of compositions of coexisting phases. Carnegie Inst Washington Yearb 72:502–505

Langmuir CH (1986) Some possible geochemical consequences of in situ fractionation in a boundary layer. EOS 67:385

Langmuir CH, Hanson GN (1981) Calculating mineral-melt equilibria with stoichiometry, mass balance, and single-component distribution coefficients. In: Newton RC, Navrotsky A, Wood BJ (eds) Thermodynamics of minerals and melts: advances in physical geochemistry 1. Springer, New York Berlin Heidelberg, pp 247–271

Lasaga AC (1981) Implication of a concentration dependent growth rate on the boundary layer crystal-melt model. Earth Planet Sci Lett 56:429–434

Lasaga AC (1982) Toward a master equation in crystal growth. Am J Sci 282:1264–1288

Lesher CE (1986) Effects of silicate liquid composition on mineral-liquid element partitioning from Soret diffusion studies. J Geophys Res 91B:6123–6141

Lesher CE, Walker D (1986a) Solution properties of silicate liquids from thermal diffusion experiments. Geochim Cosmochim Acta 50:1397–1411

Lesher CE, Walker D (1986b) Chemical diffusivities of natural silicate liquids from thermal (Soret) diffusion studies. EOS 67:409

Marvin UB, Walker D (1985) A transient heating event in the history of a highland troctolite from Apollo 12 soil 12033. Proc Lunar Planet Sci Conf 15th Part 2, J Geophys Res Suppl 90:C412–C429

Morse SA (1980) Basalts and phase diagrams: an introduction to the quantitative use of phase diagrams in igneous petrology. Springer, Berlin Heidelberg New York, p 493

Morse SA (1986) Convection in aid of adcumulus growth. J Petrol 27:1183–1214

Nelson SA, Carmichael ISE (1979) Partial molar volumes of oxide components in silicate liquids. Contrib Mineral Petrol 71:117–124

Osborn EF, Tait DB (1952) The system anorthite-diopside-albite. Am J Sci Bowen Vol 250A, pp 413–433

Roeder PL, Emslie RF (1970) Olivine-liquid equilibrium. Contrib Mineral Petrol 29:275–289

Ryerson FJ, Hess PC (1978) Implications of liquid-liquid distribution coefficients to mineral-liquid partitioning. Geochim Cosmochim Acta 42:921–932

Ryerson FJ, Watson EB (1987) Rutile saturation in magmas: implications for Ti–Nb–Ta depletion in island-arc basalts. Earth Planet Sci Lett 86:225–239

Sack RO, Walker D, Carmichael ISE (1987) Experimental petrology of alkalic lavas constraints on cotectics of multiple saturation in natural basic liquids. Contrib Mineral Petrol 96:1–23

Sato H (1974) Diffusion coronas around quartz xenocrysts in andesite and basalt from Tertiary volcanic region in northeastern Shikoku, Japan. Contrib Mineral Petrol 50:49–64

Schairer JF, Yoder HS (1960) The nature of residual liquids from crystallization, with data on the system nepheline-diopside-silica. Am J Sci 258A:273–283

Shewmon PG (1963) Diffusion in solids. McGraw-Hill, New York, p 203

Shimizu N (1981) Trace element incorporation into growing augite phenocryst. Nature 289:575–577

Shimizu N, Hart SR (1982) Application of the ion microprobe to geochemistry and cosmochemistry. Ann Rev Earth Planet Sci 10:483–526

Smith VG, Tiller WA, Rutter JW (1955) A mathematical analysis of solute redistribution during solidification. Can J Phys 33:723–745

Tsuchiyama A (1985a) Dissolution kinetics of plagioclase in the melt of system diopside-albite-anorthite and origin of dusty plagioclase in andesites. Contrib Mineral Petrol 89:1–16

Tsuchiyama A (1985b) Partial melting kinetics of plagiocalse-diopside pairs. Contrib Mineral Petrol 91:12–23

Tsuchiyama A, Takahashi E (1983) Melting kinetics of a plagioclase feldspar. Contrib Mineral Petrol 84:345–354

Walker D, Shibata T, DeLong SE (1979) Abyssal tholeiites from the Oceanographer Fracture Zone. Contrib Mineral Petrol 70:111–125

Walker D, Kiefer WS (1985) Xenolith digestion in large magma bodies. Proc Lunar Planet Sci Conf 15th Part 2, J Geophys Res Suppl 90:C585–C590

Watson EB (1976) Two-liquid partitioning coefficients: experimental data and geochemical implications. Contrib Mineral Petrol 56:119–134

Watson EB (1982a) Basalt contamination by continental crust: some experiments and models. Contrib Mineral Petrol 80:73–87

Watson EB (1982b) Melt infiltration and magma evolution. Geology 10:236–240

Weaver JS, Langmuir CH (1989) Calculation of mineral-melt equilibrium. Comput Geosci (in press)

Received May 9, 1988/Accepted March 16, 1989
Editorial responsibility: I.S.E. Carmichael